ACTIVE FIRES

VISIBLE/INFRARED IMAGER/RADIOMETER SUITE ALGORITHM THEORETICAL BASIS DOCUMENT

Version 5: March 2002

Shawn W. Miller
Quanhua Liu

RAYTHEON COMPANY
Information Technology and Scientific Services
4400 Forbes Boulevard
Lanham, MD 20706

SRBS Document #: Y3252

APPLICATION: ACTIVE FIRES

Doc No: Y3252

Version: 5

Revision: 0

	Function	Name	Signature	Date
Prepared by	Algorithm Developer	S. MILLER		1/18/02
Approved by	Relevant IPT Lead	S. MILLER		1/18/02
Reviewed by	Reviewer	K. JENSEN		1/25/02
Approved by	Chief Scientist	S. MILLER		2/01/02
Released by	Algorithm Lead	P. KEALY		2/15/02

TABLE OF CONTENTS

Page

LIST OF FIGURES iii

LIST OF TABLES v

GLOSSARY OF ACRONYMS vii

ABSTRACT ix

1.0 INTRODUCTION 1
- 1.1 PURPOSE 1
- 1.2 SCOPE 1
- 1.3 VIIRS DOCUMENTS 2
- 1.4 REVISION HISTORY 3

2.0 EXPERIMENT OVERVIEW 5
- 2.1 OBJECTIVES OF ACTIVE FIRES RETRIEVALS 5
- 2.2 INSTRUMENT CHARACTERISTICS 8
- 2.3 RETRIEVAL STRATEGY 14

3.0 ALGORITHM DESCRIPTION 15
- 3.1 PROCESSING OUTLINE 15
- 3.2 ALGORITHM INPUT 16
  - 3.2.1 VIIRS Data 16
  - 3.2.2 Non-VIIRS Data 16
- 3.3 THEORETICAL DESCRIPTION OF ACTIVE FIRES RETRIEVALS 16
  - 3.3.1 Physics of the Problem 16
    - 3.3.1.1 Spectral Characteristics of Fires 17
    - 3.3.1.2 Historical Development of Fire Products 25
  - 3.3.2 Mathematical Description of VIIRS Approach 28
    - 3.3.2.1 Fire Detection 28
    - 3.3.2.2 Subpixel Average Fire Temperature and Subpixel Fire Area 30
    - 3.3.2.3 Saturation Handling 32
    - 3.3.2.4 Burn Scar Detection 35
- 3.4 ALGORITHM SENSITIVITY STUDIES 36
  - 3.4.1 EDR Requirements 37
  - 3.4.2 Performance Metrics 38

3.4.3 Individual Error Sources for Investigation 39
3.4.4 Case Study (Fire Detection) 42
3.5 PRACTICAL CONSIDERATIONS 48
3.5.1 Numerical Computation Considerations 48
3.5.2 Programming and Procedural Considerations 48
3.5.3 Configuration of Retrievals 49
3.5.4 Quality Assessment and Diagnostics 49
3.5.5 Exception Handling 49
3.6 ALGORITHM VALIDATION 49
4.0 ASSUMPTIONS AND LIMITATIONS 51
4.1 ASSUMPTIONS 51
4.2 LIMITATIONS 51
5.0 REFERENCES 53

LIST OF FIGURES

Page

Figure 1. Forest fire altering the landscape (from www.cnn.com). 5

Figure 2. The global distribution of active vegetation fires as derived from NOAA-AVHRR satellite data for April 1, 1999 (from NOAA web site). 6

Figure 3. GOES-8 visible/IR image used to detect fires (red indicates active fires). From NOAA web site. 7

Figure 4. Sample output from the MODIS Rapid Response System from September 2001 (available as http://rapidfire.sci.gsfc.nasa.gov/images/PDFs/Global_9-2001.jpg). 8

Figure 5. Summary of VIIRS design concepts and heritage. 10

Figure 6. VIIRS detector footprint aggregation scheme for building "pixels." The numbers shown here are approximate. 10

Figure 7. Benefits of VIIRS aggregation scheme in reducing pixel growth at edge of scan. 11

Figure 8. VIIRS spectral bands, visible and near infrared (VNIR). 12

Figure 9. VIIRS spectral bands, shortwave infrared (SWIR). 12

Figure 10. VIIRS spectral bands, midwave infrared (MWIR). 13

Figure 11. VIIRS spectral bands, longwave infrared (LWIR). 13

Figure 12. Processing architecture for Active Fires Application. 15

Figure 13. Radiance characteristics of fires in the midwave infrared (MWIR) portion of the spectrum, for nighttime conditions. 17

Figure 14. Active fires response of VIIRS band M7. 18

Figure 15. Active fires response of VIIRS band M8. 19

Figure 16. Active fires response of VIIRS band M10. 20

Figure 17. Active fires response of VIIRS band M11. 21

Figure 18. Active fires response of VIIRS band M13. 22

Figure 19. Active fires response of VIIRS band M15. 23

Figure 20. Idealized VIIRS band behavior beyond specified maximum temperature for fire temperature/area measurement (actual instrument performance will fall somewhere short of this illustration due to limitations of the realized DN range). 34

Figure 21. Wild fires in the Idaho/Montana area on August 29, 2000. 42

Figure 22. Fire polygons created by U.S. Forest Service for wild fires up to October 26, 2000. 43

Figure 23. Step-by-step performance of VIIRS fire detection algorithm for Idaho/Montana case study. 44

Figure 24. Step-by-step performance of Li et al. (2000) fire detection algorithm for Idaho/Montana case study. 45

Figure 25. Step-by-step performance of Gong et al. (2001) fire detection algorithm for Idaho/Montana case study. 46

LIST OF TABLES

Page

Table 1. Component products of the Active Fires Application. 1

Table 2. VIIRS band saturation characteristics relevant to Active Fires. 11

Table 3. VIIRS bands used for Active Fires Application. 14

Table 4. Algorithm trades conducted by Raytheon for the Hazard Support System (HSS). 28

Table 5. VIIRS SRD prescribed requirements for the Active Fires product (TBD=to be determined; TBR=to be reviewed). Minimum area requirement has since increased to 1000 square meters. 38

Table 6. Comparison of three fire detection algorithms tested in case study. 43

Table 7. Quantitative assessment of fire detection algorithms' performance in case study. 47

GLOSSARY OF ACRONYMS

ASTER	Advanced Spaceborne Thermal Emission and Reflection Radiometer
ATB	Algorithm Theoretical Basis
ATBD	Algorithm Theoretical Basis Document
AVHRR	Advanced Very High Resolution Radiometer
DoD	Department of Defense
EDR	Environmental Data Record
EOS	Earth Observing System
GIFOV	Ground Instantaneous Field of View
GMS	Geostationary Meteorological Satellite
GOES	Geostationary Operational Environmental Satellite
GWSR	Gridded Weekly Surface Reflectance
HCS	Horizontal Cell Size
HSR	Horizontal Spatial Resolution
HSS	Hazard Support System
IP	Intermediate Product
IPO	Integrated Program Office
LQF	Land Quality Flag(s)
LWIR	Long Wave Infrared
MODIS	Moderate Resolution Imaging Spectroradiometer
MTF	Modulation Transfer Function
MWIR	Mid Wave Infrared
NASA	National Aeronautics and Space Administration
NASA/GSFC	NASA Goddard Space Flight Center
NCEP	National Centers for Environmental Prediction
NDVI	Normalized Difference Vegetation Index
NIR	Near Infrared
NOAA	National Oceanic and Atmospheric Administration
NPOESS	National Polar-orbiting Operational Environmental Satellite System
NPP	NPOESS Preparatory Project
OLS	Operational Linescan System
PF	Potential Fire
PFM	Protoflight Model (MODIS)
RDR	Raw Data Record
SAFARI	Southern African Regional Science Initiative
SBRS	Santa Barbara Remote Sensing
SCAR	Smoke, Clouds, and Radiation
SDR	Sensor Data Record
SDSM	Solar Diffuser Stability Monitor
SNR	Signal-to-Noise Ratio

SRD	Sensor Requirements Document
SSAI	Science Systems and Applications, Inc.
SST	Sea Surface Temperature
SWIR	Short Wave Infrared
TIROS	Television Infrared Observation Satellite
TOA	Top of Atmosphere
VIIRS	Visible/Infrared Imager/Radiometer Suite

ABSTRACT

Active Fires is one of more than two dozen products explicitly required to be derived from the Visible/Infrared Imager/Radiometer Suite (VIIRS) sensor slated to fly onboard the National Polar-orbiting Operational Environmental Satellite System (NPOESS), which is scheduled for launch in 2008. The requirements for the VIIRS EDRs are described in detail in the VIIRS Sensor Requirements Document (SRD). These requirements form the foundation from which both the algorithms and the sensor are designed and built. A revised version of the SRD was released in November 1999, detailing a set of new requirements targeted toward the NPOESS Preparatory Project (NPP), a National Aeronautics and Space Administration (NASA) endeavor to build upon the MODIS heritage beginning in 2005. The Active Fires environmental data record (EDR) was added to the VIIRS SRD at that time. The most recent version of the VIIRS SRD remapped Active Fires to the status of an Application, under the heading of the Surface Type EDR. The Active Fires Application will consist of three distinct components: the detection of a fire or fires within a given geolocated VIIRS pixel; the subpixel average temperature of the fire or fires detected; and the subpixel area of the fire or fires detected. These latter two components represent a significant step forward in operational remote sensing of fires from space. This document includes a thorough description of the algorithm used to retrieved the product components listed above. Fire detection is based on contextual analysis; fire temperature and area retrieval are based on an extension of the two-band technique described in Dozier (1981). Additionally, Raytheon proposes the addition of a burn scar detection parameter to the product output, following the MODIS heritage.

1.0 INTRODUCTION

1.1 PURPOSE

This algorithm theoretical basis document (ATBD) describes the algorithms used to retrieve the Active Fires Application for the Visible/Infrared Imager/Radiometer Suite (VIIRS). Active Fires consists of three distinct components: detection of fires; subpixel average temperature of detected fires; and subpixel area of detected fires. This document will describe the required inputs, a theoretical description of the algorithms, the sources and magnitudes of the errors involved, practical considerations for post-launch implementation, and the assumptions and limitations associated with the products. Table 1 summarizes the three components of the Active Fires Application. SRD is an acronym for the VIIRS Sensor Requirements Document (IPO, 2000).

Table 1. Component products of the Active Fires Application.

Component	Description	Purpose
Fire Detection	Flagging of a given geolocated VIIRS pixel to indicate the presence of an active fire or fires within, which is assigned to the center latitude and longitude of the pixel.	Operational monitoring of fires, launching point for evaluation of more detailed parameters which serve both operational and research purposes.
Subpixel Average Fire Temperature	The average temperature of all surfaces within a fire-detected pixel that are overlain by an active fire or fires.	Feeds into tactical issues for handling of fires, aids the computation of energy/aerosol/carbon fluxes into the atmosphere
Subpixel Fire Area	The projection of the total area of all surfaces within a fire-detected pixel that are overlain by an active fire or fires onto a plane perpendicular to the normal vector at the center of the pixel.	Feeds into tactical issues for handling of fires, aids the computation of energy/aerosol/carbon fluxes into the atmosphere
Burn Scar Detection	Flagging of a given geolocated VIIRS pixel to indicate that it is dominated by burned vegetation from recent active fires.	Monitoring of forest and agricultural vegetation cover, assistance in assessing carbon exchange between surface and atmosphere

1.2 SCOPE

This document covers the algorithm theoretical basis (ATB) for the operational retrieval of the Active Fires Application. Any derived products beyond the three components of Active Fires will not be discussed beyond brief mention. The exact structure of the algorithms for the Active Fires Application may change during the developmental phase of this experiment; this document

will be revised accordingly to match those changes. Only the algorithms that will be implemented for routine operational processing will be preserved in the final release of this document.

Section 1 describes the purpose and scope of this document; it also includes a listing of VIIRS documents that will be cited in the following sections. Section 2 provides a brief overview of the motivation for the Active Fires algorithm, including the objectives of the retrievals, the currently designed VIIRS instrument characteristics, and the strategy for retrieval of the Active Fires product. Section 3 contains the essence of this document—a complete description of the Active Fires Application and its components. Consideration is given to the overall structure, the required inputs, a theoretical description of the algorithm, assessment of the error budget, results of ongoing sensitivity studies, practical implementation issues, and recommendations for product validation. Section 4 provides an overview of the constraints, assumptions and limitations associated with the Active Fires Application, and Section 5 contains a listing of non-VIIRS references cited throughout the course of this document.

1.3 VIIRS DOCUMENTS

Reference to VIIRS documents within this ATBD will be indicated by an italicized Raytheon Santa Barbara Remote Sensing (SBRS) official Y-number in brackets, e.g., *[Y2388]*.

Y2388 VIIRS Aerosol Optical Thickness and Aerosol Particle Size Parameter ATBD

Y2390 VIIRS Suspended Matter ATBD

Y2393 VIIRS Cloud Effective Particle Size and Cloud Optical Thickness ATBD

Y2400 VIIRS Vegetation Index ATBD

Y2402 VIIRS Surface Type ATBD

Y2411 VIIRS Surface Reflectance ATBD

Y2412 VIIRS Cloud Mask ATBD

Y2468 VIIRS Operations Concept Document

Y2469 VIIRS Context Level Software Architecture

Y2470 VIIRS Interface Control Document (ICD)

Y2474 VIIRS Land Module Level Software Architecture

Y2483 VIIRS Land Module Level Detailed Design

Y3236 VIIRS Software Integration and Test Plan

Y3237 VIIRS Algorithm Verification and Validation Plan

Y3251 VIIRS Precipitable Water ATBD

Y3257 VIIRS Computer Resources Requirements Document

Y3261 VIIRS Radiometric Calibration ATBD

Y3270 VIIRS System Verification and Validation Plan

Y3279 VIIRS Land Module Level Interface Control Document

Y3283 VIIRS Active Fires Unit Level Detailed Design

Y6635 VIIRS Algorithm Software Development Plan

Y6661 VIIRS Algorithm Software Maturity Assessment

Y7040 VIIRS Algorithm/Data Processing Technical Report

Y7051 VIIRS Earth Gridding ATBD

SS154650 VIIRS System Specification

PS154650 VIIRS Sensor Specification

PS154640 VIIRS Algorithm Specification

1.4 REVISION HISTORY

This is the third working version of this document, however it is labeled Version 5 to match it with the delivery of the other VIIRS ATBDs (Active Fires was a late introduction to the VIIRS requirements). The current version is dated March 2002. Version 4 was dated May 2001. The first working version, Version 3, was dated May 2000. The authors would like to thank Luke Flynn for a number of insightful discussions in Phase I algorithm development, and Eric Vermote and Louis Giglio for further guidance in Phase II. This document has been significantly revised since Version 4. The primary areas in which changes have been made are:

1) Updates of VIIRS band descriptions where appropriate

2) Updated software architecture snapshot (see *[Y2474]* for latest version)

3) Refined description of fire detection algorithm logic (Section 3.3.2.1)

4) Updated summary of saturation handling (Section 3.3.2.3)

5) Added discussion of approach for burn scar detection (Section 3.3.2.4)

6) Results from a single case study (Section 3.4.4)

7) Updated discussion of quality flags (discussed in *[Y2411]* for all land products)

2.0 EXPERIMENT OVERVIEW

2.1 OBJECTIVES OF ACTIVE FIRES RETRIEVALS

As pointed out in the MODIS Fire Products ATBD (Kaufman and Justice, 1998), fire is an important process in many terrestrial biomes, and the release of gases and particulate matter during biomass burning is an important contributor to the chemical reactions and physical processes taking place in the atmosphere. Fire is a significant factor in the ecology of savannas, boreal forests, and tundra, and it plays a central role in deforestation in tropical and sub-tropical regions.

Severe fires have large impacts on climate changes. Fires change the physical state of the vegetation, releasing a variety of greenhouse gases into the atmosphere. There is presently great uncertainty as to the magnitude of the sources and sinks of these greenhouse gases. The release of chemically reactive gases during biomass burning strongly influences chemical processes within the troposphere. It is estimated that annual biomass burning may be associated with 38% of the ozone in the troposphere; 32% of global carbon monoxide; more than 20% of the world's hydrogen, non-methane hydrocarbons, methyl chloride and oxides of nitrogen; and approximately 39% of the particulate organic carbon (Levine, 1991; Andreae, 1991; Kaufman *et al*., 1998a,b).

Satellite data have been widely applied to the monitoring of fires over vegetated land, especially over forests. The Advanced Very High Resolution Radiometer (AVHRR), Geostationary Operational Environmental Satellite (GOES), and Geostationary Meteorological Satellite (GMS) have all been successfully utilized for monitoring severe fires in California, Brazil, China, and Indonesia. The remote sensing of fire aftermaths has also received considerable attention, as fires have a propensity for making abrupt, large-scale changes in the vegetation index (see Figure 1).

Figure 1. Forest fire altering the landscape (from www.cnn.com).

The global distribution of active vegetation fires can be derived from AVHRR data, as seen in Figure 2. The area of an active fire can be smaller than a square meter or larger than 100 square kilometers.

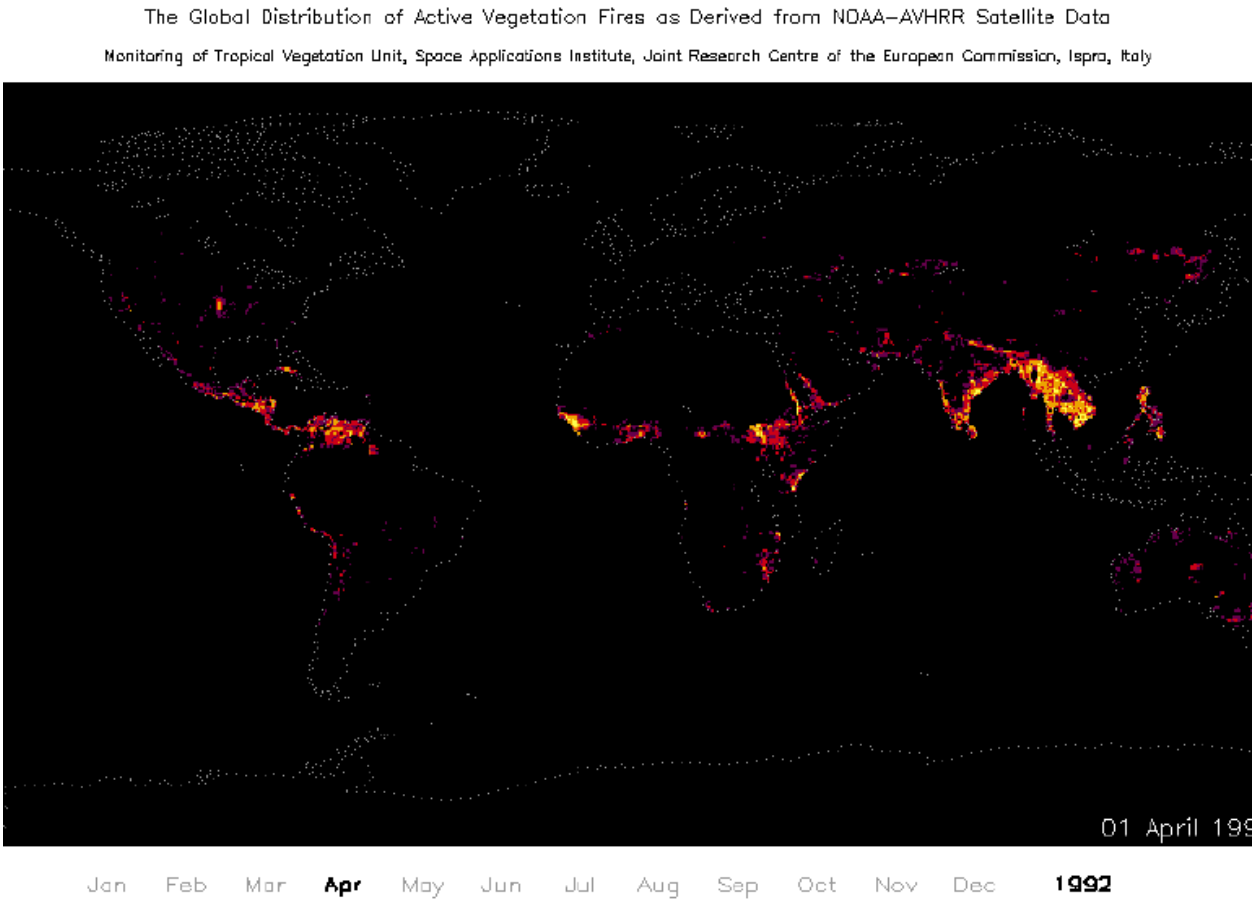

Figure 2. The global distribution of active vegetation fires as derived from NOAA-AVHRR satellite data for April 1, 1999 (from NOAA web site).

Figure 3 shows the capabilities of GOES for fire detection. Active fires are highlighted based on data from the midwave infrared (MWIR) band at 3.9 µm. Smoke from the fires can be seen from the visible band.

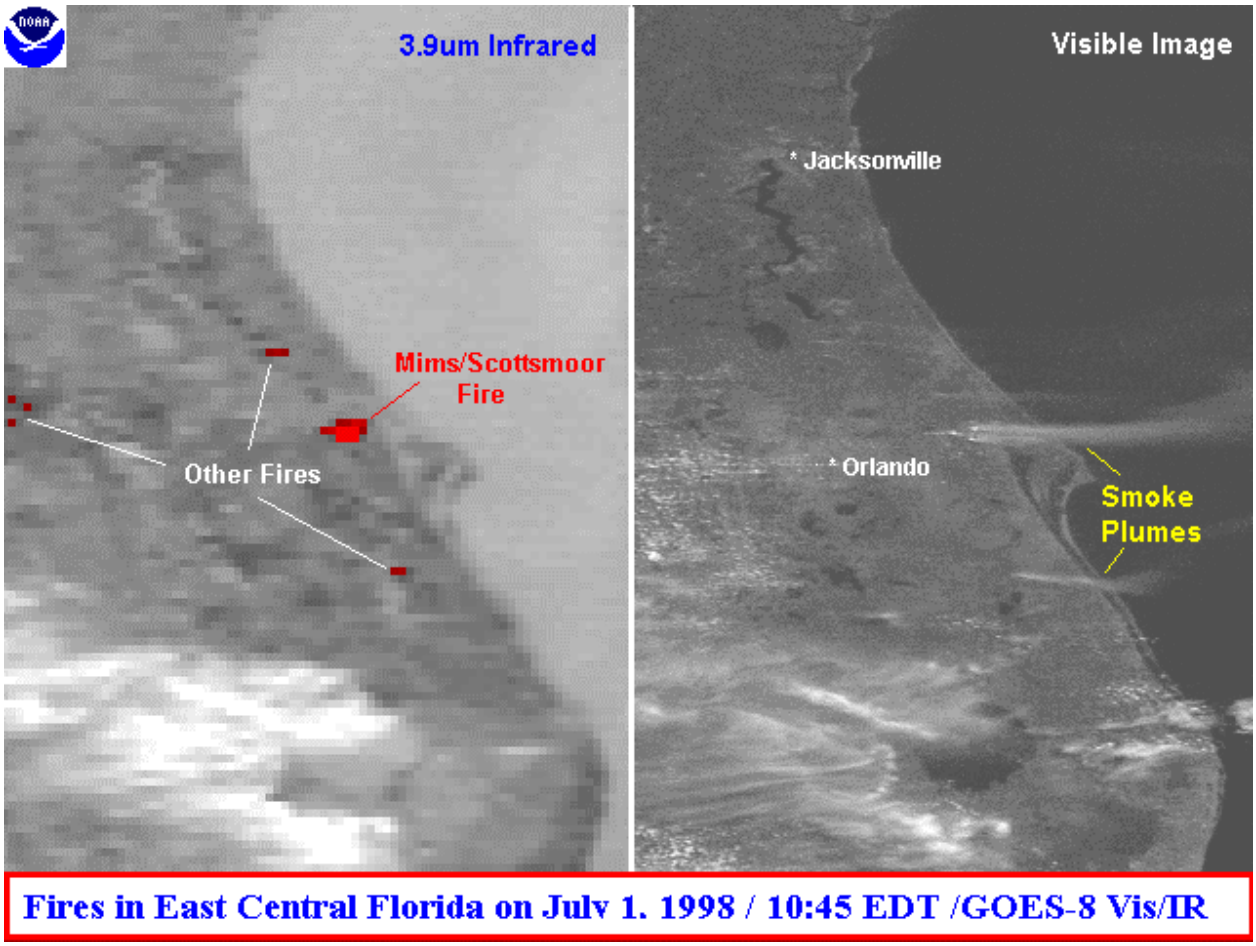

Figure 3. GOES-8 visible/IR image used to detect fires (red indicates active fires). From NOAA web site.

The latest advancements in automated fire detection are illustrated in Figure 4, which shows a sample global fire detection map for September 2001, from the MODIS Rapid Response System (http://rapidfire.sci.gsfc.nasa.gov). VIIRS will build directly on the achievements of the MODIS algorithm development team.

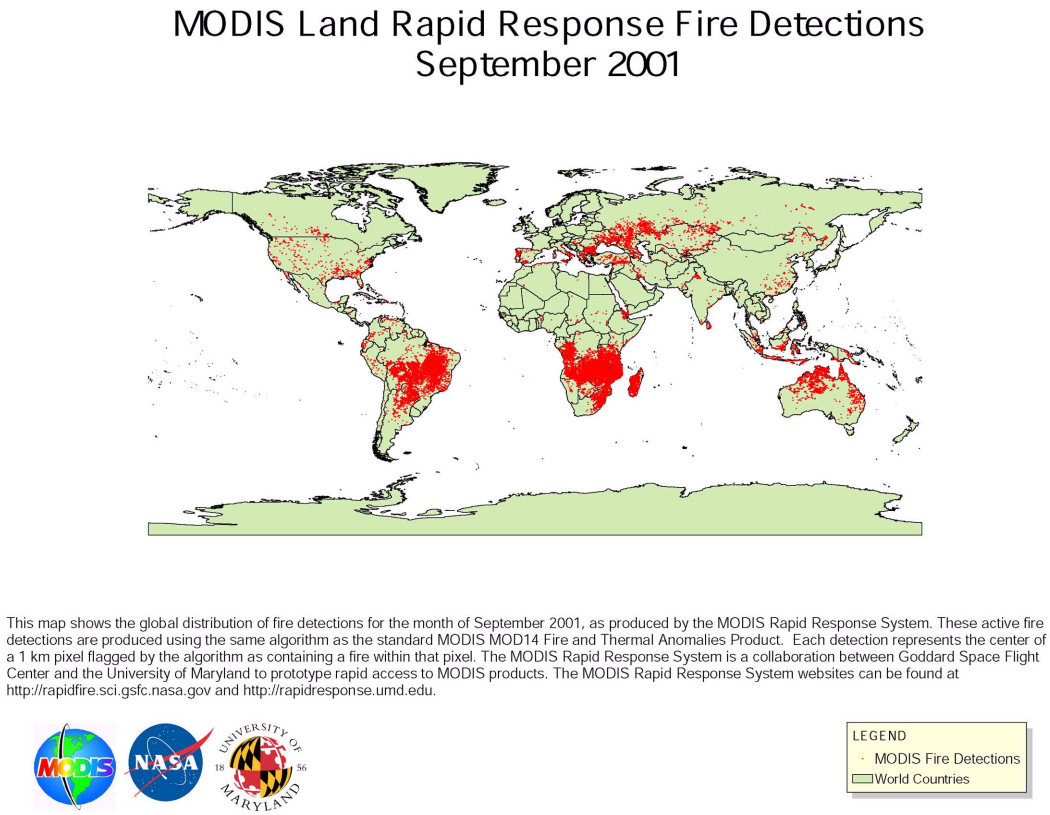

Figure 4. Sample output from the MODIS Rapid Response System from September 2001 (available as http://rapidfire.sci.gsfc.nasa.gov/images/PDFs/Global_9-2001.jpg).

2.2 INSTRUMENT CHARACTERISTICS

The VIIRS instrument will now be briefly described to clarify the context of the descriptions of the Active Fires Application presented in this document. VIIRS can be pictured as a convergence of three existing sensors, two of which have seen extensive operational use at this writing.

The Operational Linescan System (OLS) is the operational visible/infrared scanner for the Department of Defense (DoD). Its unique strengths are controlled growth in spatial resolution through rotation of the ground instantaneous field of view (GIFOV) and the existence of a low-level light sensor (LLLS) capable of detecting visible radiation at night. OLS has primarily served as a data source for manual analysis of imagery. The Advanced Very High Resolution Radiometer (AVHRR) is the operational visible/infrared sensor flown on the National Oceanic and Atmospheric Administration (NOAA) Television Infrared Observation Satellite (TIROS-N) series of satellites (Planet, 1988). Its unique strengths are low operational and production cost and the presence of five spectral channels that can be used in a wide number of combinations to produce operational and research products. In December 1999, the National Aeronautics and Space Administration (NASA) launched the Earth Observing System (EOS) morning satellite,

Terra, which includes the Moderate Resolution Imaging Spectroradiometer (MODIS). This sensor possesses an unprecedented array of thirty-two spectral bands at resolutions ranging from 250 m to 1 km at nadir, allowing for currently unparalleled accuracy in a wide range of satellite-based environmental measurements.

VIIRS will reside on a platform of the National Polar-orbiting Operational Environmental Satellite System (NPOESS) series of satellites. It is intended to be the product of a convergence between DoD, NOAA and NASA in the form of a single visible/infrared sensor capable of satisfying the needs of all three communities, as well as the research community beyond. As such, VIIRS will require three key attributes: high spatial resolution with controlled growth off nadir, minimal production and operational cost, and a large number of spectral bands to satisfy the requirements for generating accurate operational and scientific products.

Figure 5 illustrates the design concept for VIIRS, designed and built by Raytheon Santa Barbara Remote Sensing (SBRS). At its heart is a rotating telescope scanning mechanism that minimizes the effects of solar impingement and scattered light. Calibration is performed onboard using a solar diffuser for short wavelengths and a V-groove blackbody source and deep space view for thermal wavelengths. A solar diffuser stability monitor (SDSM) is also included to track the performance of the solar diffuser. The nominal altitude for NPOESS will be 833 km. The VIIRS scan will extend to 56 degrees on either side of nadir.

The VIIRS SRD places explicit requirements on spatial resolution for the Imagery EDR. Specifically, the horizontal spatial resolution (HSR) of bands used to meet threshold Imagery EDR requirements must be no greater than 400 m at nadir and 800 m at the edge of the scan. This led to the development of a unique scanning approach which optimizes both spatial resolution and signal to noise ratio (SNR) across the scan. The concept is summarized in Figure 6 for the imagery bands; the nested lower resolution radiometric bands follow the same paradigm at exactly twice the size. The VIIRS detectors are rectangular, with the smaller dimension projecting along the scan. At nadir, three detector footprints are aggregated to form a single VIIRS “pixel.” Moving along the scan away from nadir, the detector footprints become larger both along track and along scan, due to geometric effects and the curvature of the Earth. The effects are much larger along scan. At around 32 degrees in scan angle, the aggregation scheme is changed from 3x1 to 2x1. A similar switch from 2x1 to 1x1 aggregation occurs at 48 degrees. The VIIRS scan consequently exhibits a pixel growth factor of only 2 both along track and along scan, compared with a growth factor of 6 along scan which would be realized without the use of the aggregation scheme. Figure 7 illustrates the benefits of the aggregation scheme for spatial resolution.

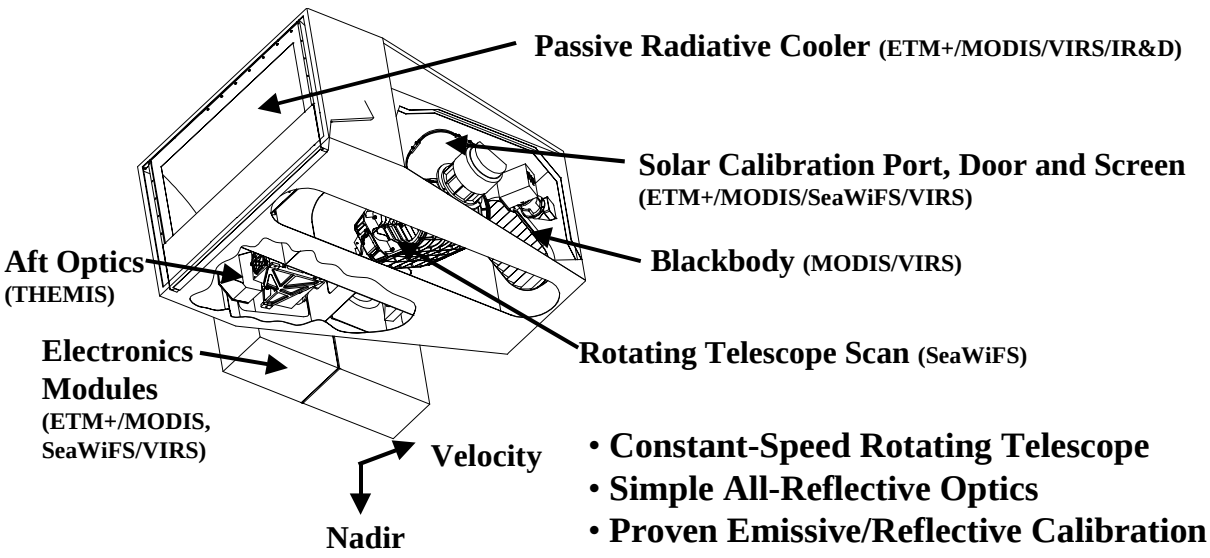

Figure 5. Summary of VIIRS design concepts and heritage.

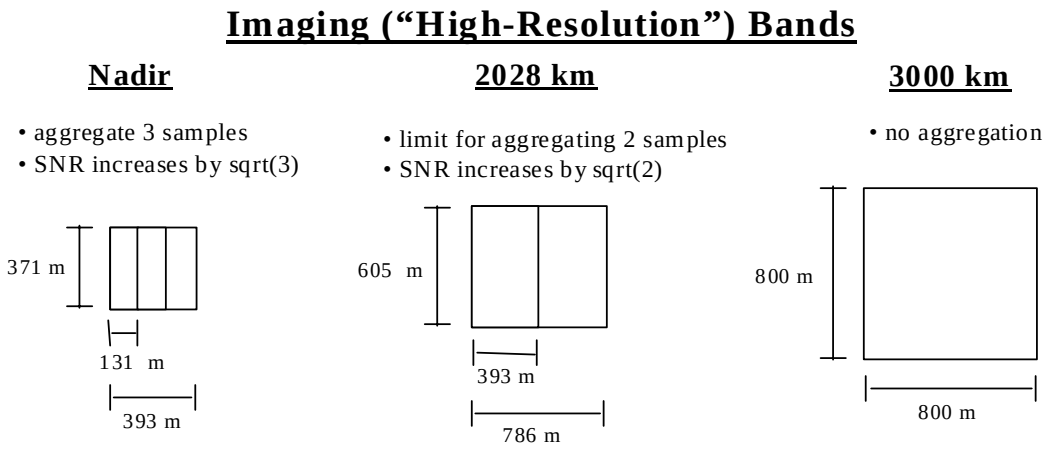

Figure 6. VIIRS detector footprint aggregation scheme for building "pixels." The numbers shown here are approximate.

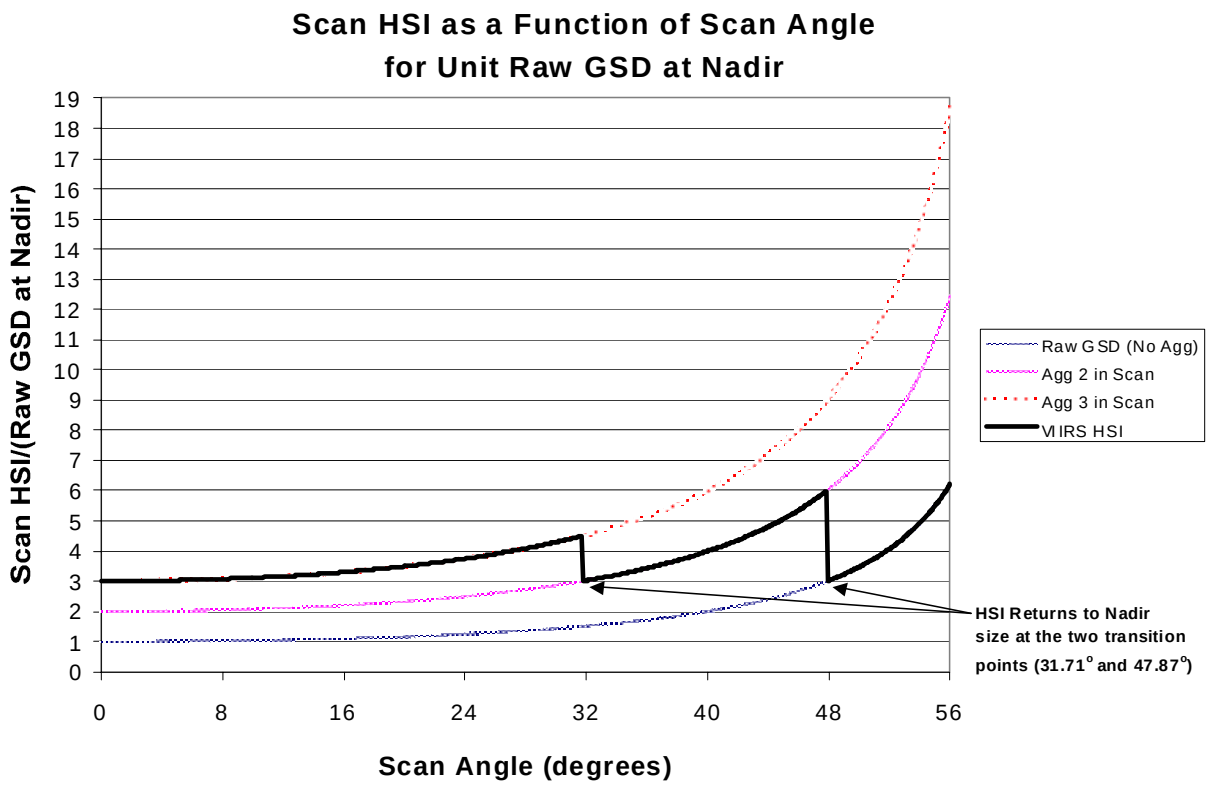

Figure 7. Benefits of VIIRS aggregation scheme in reducing pixel growth at edge of scan.

This scanning approach is extremely beneficial for the retrieval of land products such as Active Fires, although the improved spatial resolution at the edge of the swath also increases the chances of band saturation compared to other instruments such as MODIS. The positioning of the VIIRS spectral bands is summarized in Figure 8 through Figure 11. Table 2 summarizes the saturation characteristics of the instrument in the bands relevant to Active Fires. "Tmax" is the saturation temperature in the band. "Lbmax" is band radiance in $Wcm^{-2}sr^{-1}$. "Lmax" is spectral radiance in $W\ m^{-2}sr^{-1}\mu m^{-1}$. "Solar" is the solar irradiance in the band ($Wm^{2}sr^{-1}\mu m^{-1}$) divided by π. "Rmax" is the reflectance obtained when dividing "Lmax" by "Solar." The issue of saturation will be addressed again in Section 3.3.2.3, as it has had a significant impact on the strategy for Active Fires algorithm development. A detailed summary of the radiometric, spatial, and spectral characteristics of VIIRS can be found in the VIIRS Sensor Specification *[PS154650]*.

Table 2. VIIRS band saturation characteristics relevant to Active Fires.

Band	Center	Width	Solar	Tmax	Lbmax	Lmax	Rmax
M7	0.8650	0.0390	310.2	**1235**	1.36E-03	348.0	1.12
M8	1.2400	0.0200	149.2	**935**	3.31E-04	165.7	1.11
M10	1.6100	0.0600	78.1	**749**	4.35E-04	72.4	0.93
M11	2.2500	0.0500	24	**577**	1.59E-04	31.8	1.32
M13	4.0500	0.1550	---	**634**	6.27E-03	404.3	---
M15	10.7625	1.0000	---	**343**	1.71E-03	17.1	---
I5	11.4500	1.9000	---	**340**	2.93E-03	15.4	---

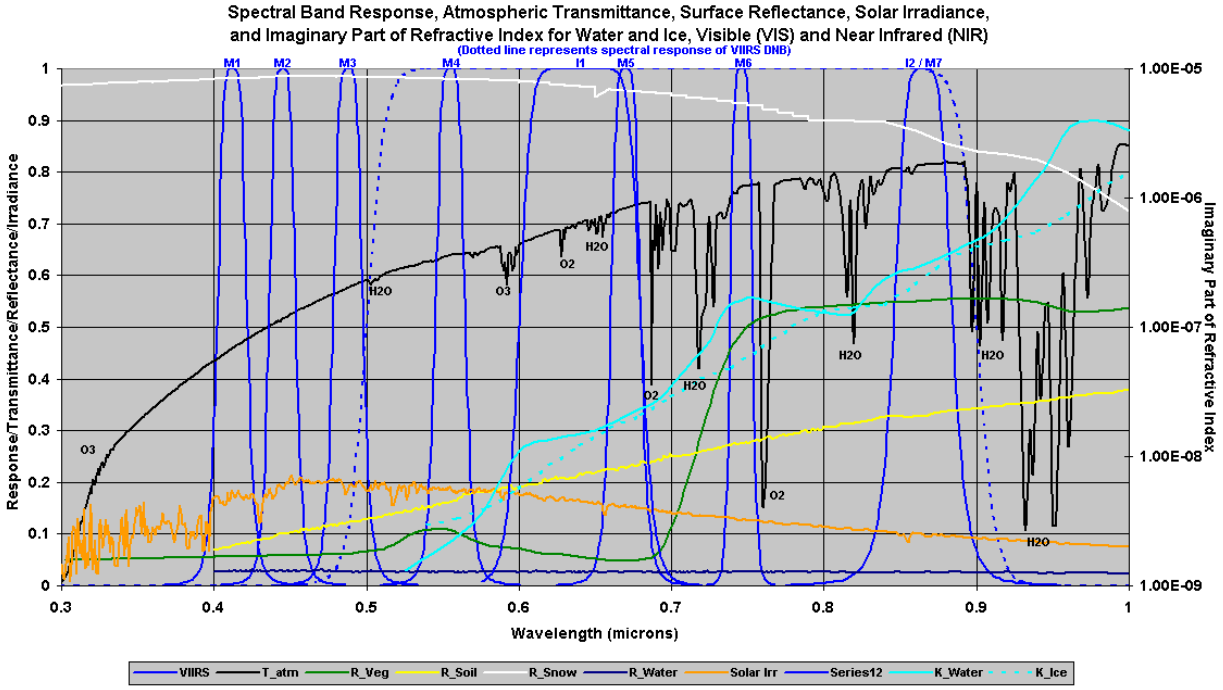

Figure 8. VIIRS spectral bands, visible and near infrared (VNIR).

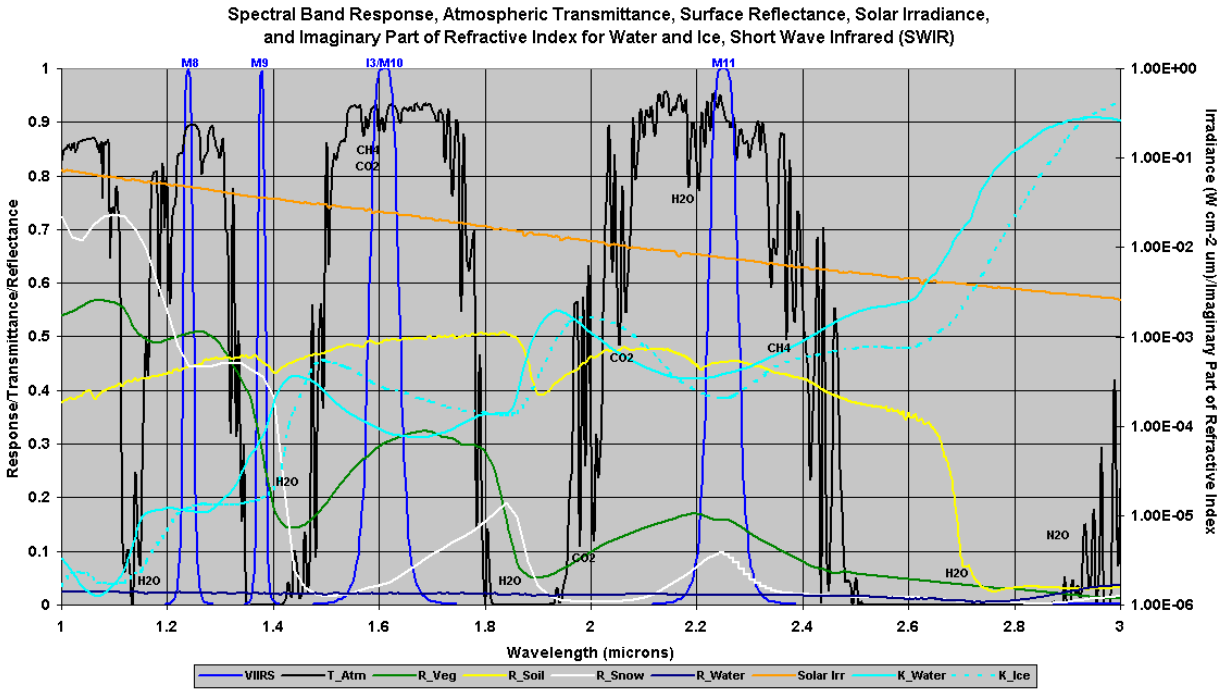

Figure 9. VIIRS spectral bands, shortwave infrared (SWIR).

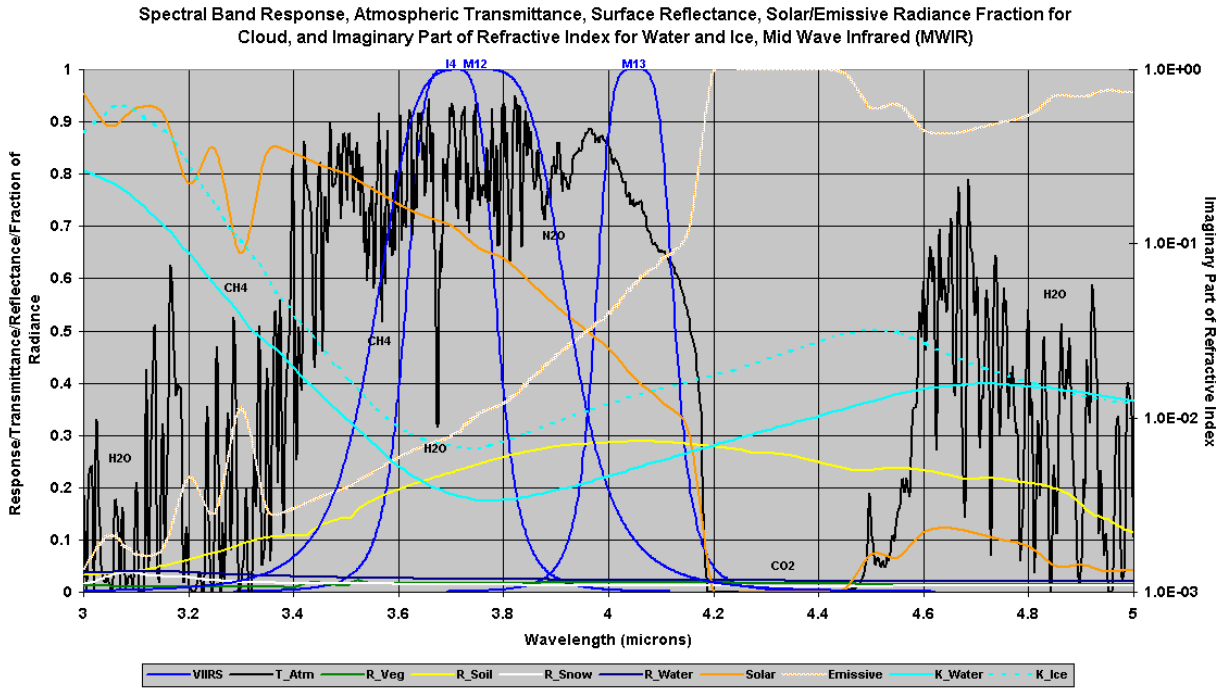

Figure 10. VIIRS spectral bands, midwave infrared (MWIR).

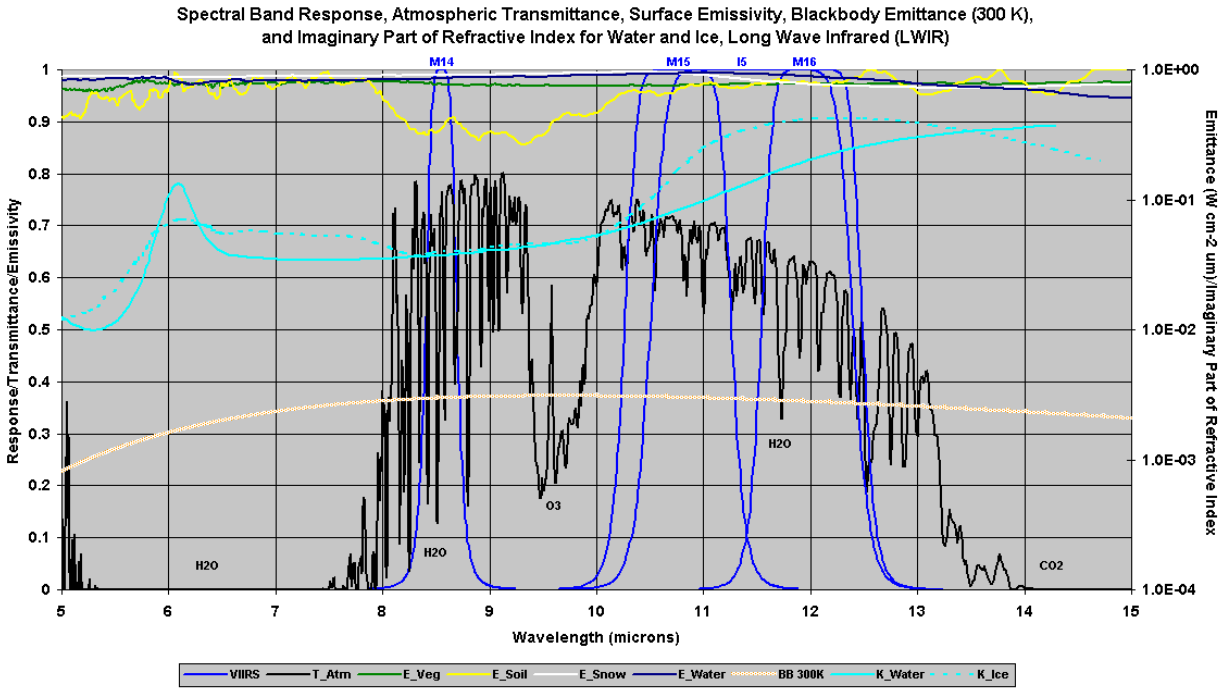

Figure 11. VIIRS spectral bands, longwave infrared (LWIR).

2.3 RETRIEVAL STRATEGY

The Active Fires product is retrieved over land surfaces, both day and night, under clear conditions. Land is defined as anything not categorized as ocean by the land/sea mask present in the VIIRS Cloud Mask output. Day is defined by a solar zenith angle of 85 degrees or less. The only difference between day and night processing is that the solar signal must be removed from the reflective bands prior to implementation of the Active Fires algorithm. This removal will take place within the Active Fires unit level code. “Clear” means that the pixel in question is classified by the VIIRS Cloud Mask as either “clear,” “probably clear,” or "probably cloudy." If the pixel is classified as "probably clear" or "probably cloudy," the VIIRS Land Quality Flag (LQF) output, appended to the Surface Reflectance IP *[Y2411]* and copied to the Active Fires Application output, will include a flag indicating possible cloud contamination. The VIIRS SRD requires Active Fires to be retrieved under conditions of “broken clouds,” however this is interpreted to mean that the pixel in question may be surrounded by cloudy pixels, yet itself is classified as “confident clear,” “probably clear,” or "probably cloudy."

The VIIRS operations concept stipulates that three nominally reflectance-based bands—M7 (865 nm), M8 (1.24 μm), and M10 (1.61 μm)—will be active both day and night to facilitate the retrieval of the Active Fires product. These bands are helpful for the measurement of fire temperature and area in instances of large and/or very hot fires, since the LWIR bands saturate in such conditions. Due to uncertainties in the use of NIR and SWIR bands, however, we are continuing to seek alternative solutions to saturation in the LWIR. This issue is discussed at length in Section 3.3.2.3. Table 3 summarizes the bands used in the retrieval of the Active Fires Application. The baseline algorithm relies on moderate resolution bands alone, which are used for both detection and the measurement of fire temperature and area. The hotter and/or larger the fire, the shorter the wavelengths necessary to retrieve its temperature and area. Retrieval of fires during the 1730 (terminator) orbit will be of great use, as this is the time during which fires typically reach their peak, after a day’s worth of solar heating.

Table 3. VIIRS bands used for Active Fires Application.

Band	Center Wavelength (μm)	Nadir resolution (m)	Usage for Active Fires
M7	0.87	750	Temperature/area measurement for very hot/large fires
M8	1.24	750	Temperature/area measurement for very hot/large fires
M10	1.61	750	Temperature/area measurement for very hot/large fires
M13	4.05	750	Detection/temperature/area measurement
M15	10.76	750	Detection/temperature/area measurement

3.0 ALGORITHM DESCRIPTION

3.1 PROCESSING OUTLINE

Figure 12 illustrates the general processing architecture for the Active Fires Application. This is only a snapshot at the writing of this document; the reader is directed to *[Y2474]* for the latest software architecture. The primary inputs are brightness temperatures from the VIIRS 750-m Earth View Sensor Data Record (SDR), particularly in VIIRS bands M7 (865 nm), M8 (1.24 µm), M10 (1.61 µm), M13 (4.05 µm), and M15 (10.76 µm). The Quarterly Surface Types IP *[Y2402]* and Vegetation Index EDR *[Y2400]* provide a characterization of the background, and the Cloud Mask IP *[Y2412]* includes sunglint detection to prevent false alarms over inland water bodies. More detail on the detection of fires, as well as the calculation of fire temperature and area, including the handling of band saturation, is provided in Section 3.3.2.

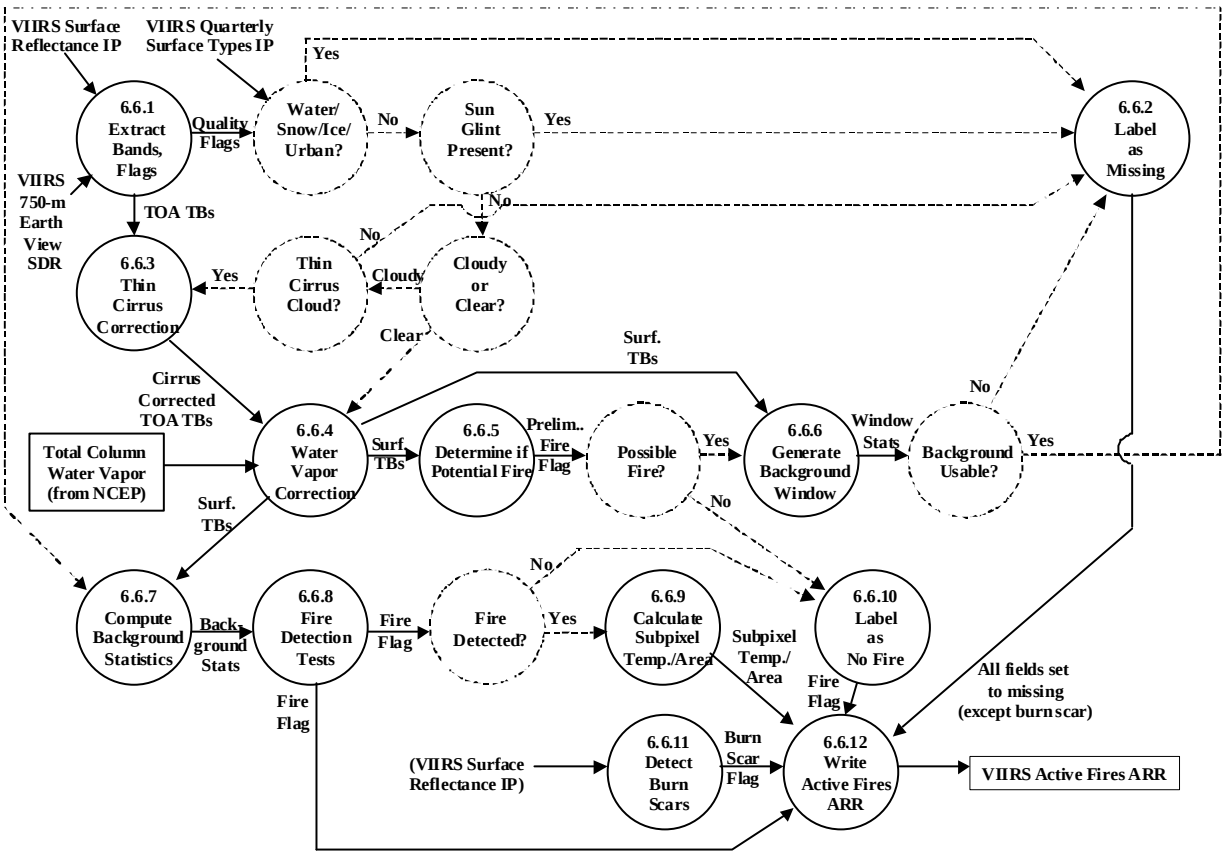

Figure 12. Processing architecture for Active Fires Application.

3.2 ALGORITHM INPUT

3.2.1 VIIRS Data

The Active Fires product requires as its most basic input the VIIRS 750-m Earth View SDR. This data flow includes both calibrated brightness temperatures in the necessary bands (M7, M8, M10, M13, M15) and required accompanying information, including solar/viewing geometry and geolocation information. The Vegetation Index EDR and Quarterly Surface Types IP provide additional information that reduces errors in the characterization of the background. The Cloud Mask IP output includes flags for clouds and sunglint. The Gridded Weekly Surface Reflectance (GWSR) IP will be required during the day, i.e., for a solar zenith angle of 85 degrees or less. This product is already being generated for the purposes of the Cloud Optical Properties EDRs. The algorithm for producing the GWSR IP is summarized in the VIIRS Earth Gridding ATBD *[Y7051]*. When band M15 saturates, it may be necessary to move into the shortwave infrared (SWIR) and possibly the near infrared (NIR) to assist in the retrieval of fire temperature and area. During the daytime, the SWIR and NIR bands are, in this context, contaminated by a solar reflective signal that depends on the surface type, solar/viewing geometry, and atmospheric conditions. The GWSR IP, together with the solar/viewing geometry for the pixel in question, may allow for algorithmic removal of this reflective signal so that the emissive signal from the fire can be isolated for fire temperature/area calculations.

The VIIRS Aerosol Optical Thickness and Aerosol Model Information IPs *[Y2388]* will be required as input to Active Fires processing, so that the effects of aerosols can be accounted for in the retrieval of surface brightness temperatures. To first order, the aerosols will tend to scatter the NIR and SWIR radiation and absorb in the MWIR and LWIR.

Finally, the Active Fires Application will require knowledge of the atmospheric water vapor present along the path between the surface and the sensor. VIIRS will be producing an EDR that supplies this information *[Y3251]*, however this EDR uses the MWIR and LWIR bands to retrieve precipitable water, and if a fire is present, the output water vapor estimation will be unreliable. Consequently, the baseline approach is to incorporate National Centers for Environmental Prediction (NCEP) analyses for column water vapor.

3.2.2 Non-VIIRS Data

As mentioned above, the only non-VIIRS input expected to be required for Active Fires processing is NCEP column water vapor.

3.3 THEORETICAL DESCRIPTION OF ACTIVE FIRES RETRIEVALS

3.3.1 Physics of the Problem

The physics underlying the retrieval of active fires is based on the enhanced thermal radiation caused by the high temperatures associated with smoldering and flaming fires. The peak of the surface emitted radiance shifts to shorter wavelengths as the surface temperature increases. The following sections detail the spectral and mathematical bases for fire retrievals.

3.3.1.1 Spectral Characteristics of Fires

Figure 13 illustrates the radiances typical of various types of fire/volcano scenarios at the Earth's surface, for nighttime conditions. The blackbody for a typical land surface temperature follows the traditional trend of increasing radiance into the longwave infrared (LWIR). A cooling lava flow is the next most similar curve, but its peak is well toward the midwave infrared (MWIR). A very active fire covering a very small portion of the pixel will exhibit a peak around 5 µm, and a larger active fire with a surrounding smoldering region extending throughout the pixel will push the peak of the blackbody curve down to 3 µm. The flaming portion of a fire can get as hot as 1800 K, at which point the blackbody curve shifts into the shortwave infrared (SWIR).

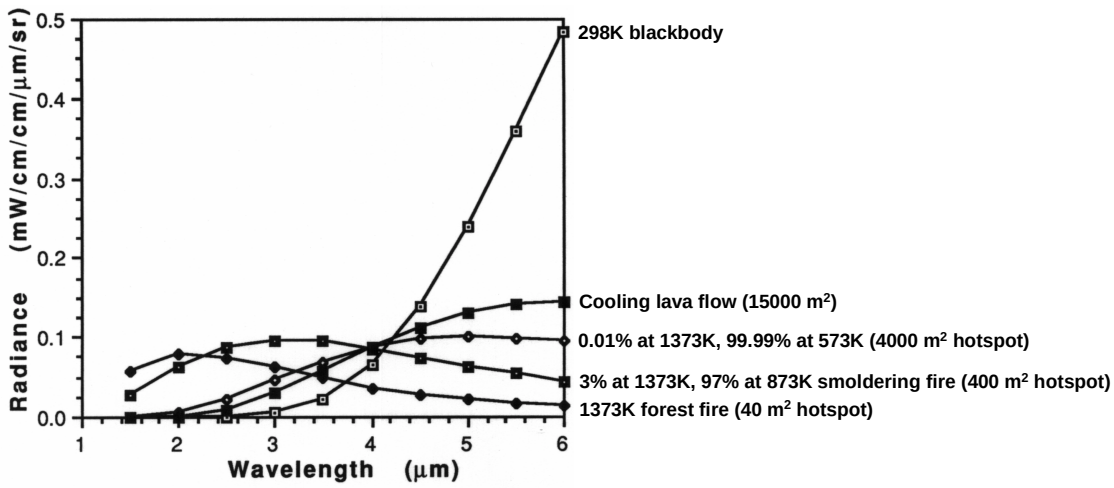

Figure 13. Radiance characteristics of fires in the midwave infrared (MWIR) portion of the spectrum, for nighttime conditions.

The sensitivity to active fires at 4.05 and 10.76 µm is different because of the different atmospheric absorption properties and the different behavior of the Planck function at the two wavelengths. As a fire becomes hotter or larger, its contribution to the total pixel radiance grows, and by Wein's displacement law it shifts into the shorter wavelengths. There are two general states of an active fire: flaming and smoldering. Flaming tends to occur around an average temperature of 1000 K, while smoldering tends to occur at a temperature of 600 K. These are merely averaged values, but they are suitable for the discussion at hand. Using these typical temperatures, one can calculate in the VIIRS bands what the maximum measurable area of smoldering or flaming fire would be for a given pixel. Figures 14 through 19 on the following several pages summarize the capabilities of the relevant VIIRS bands. Band M11 (2.25 µm) is included to illustrate why it is no longer being considered for use in the event that SWIR bands are utilized. Each figure illustrates the brightness temperature in a given band corresponding to the fire temperature along the y-axis and the fire area across the x-axis. The ranges of these axes essentially enclose the measurement range from the VIIRS system specification. Gray-shaded areas on the plots indicate the band has saturated. The contours are shown in increments of 100 K, starting at 300 K (the assumed background temperature). The "wavy" nature of some of the contour lines is an artifact of the contour plotting process.

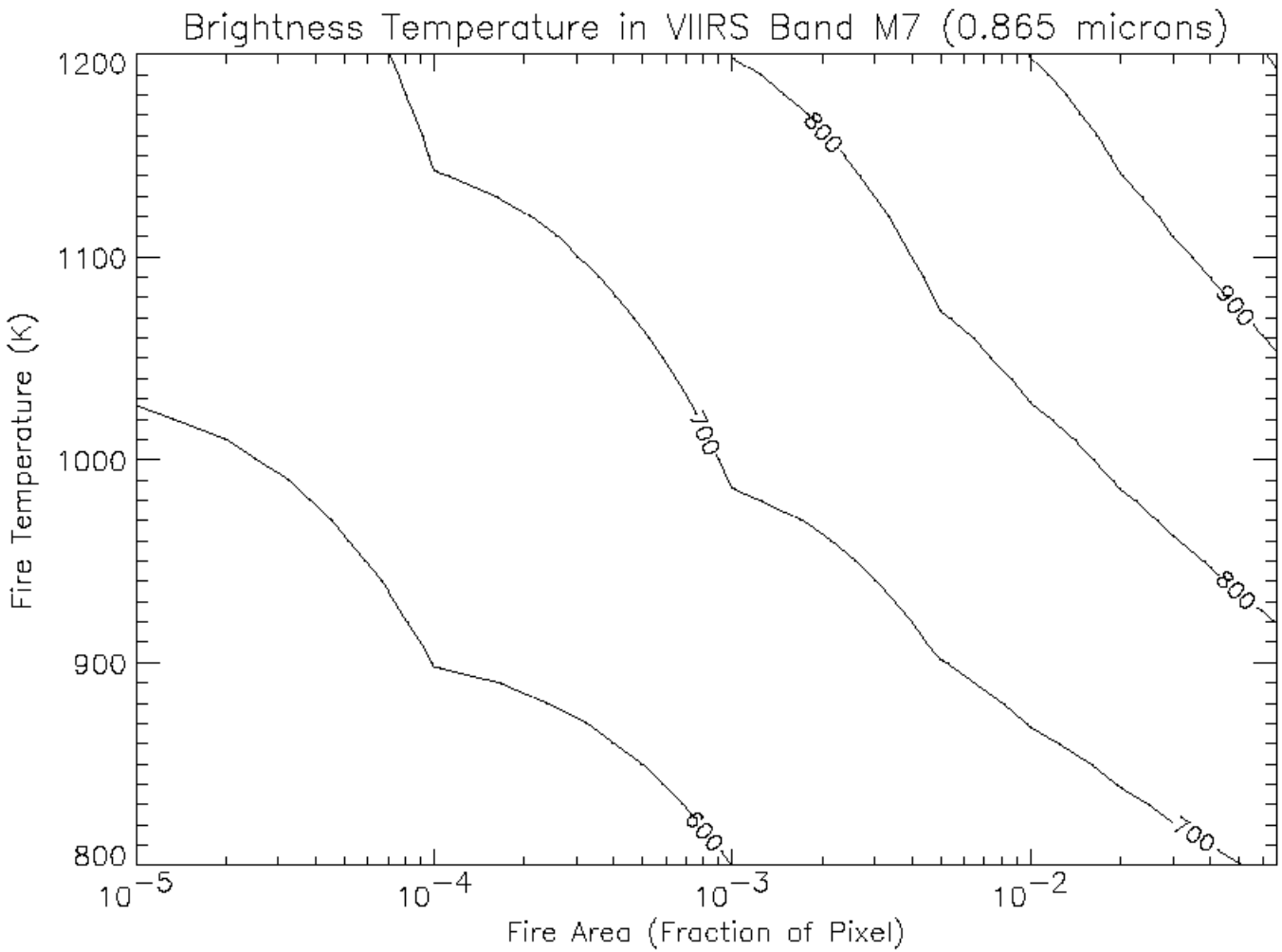

Figure 14. Active fires response of VIIRS band M7.

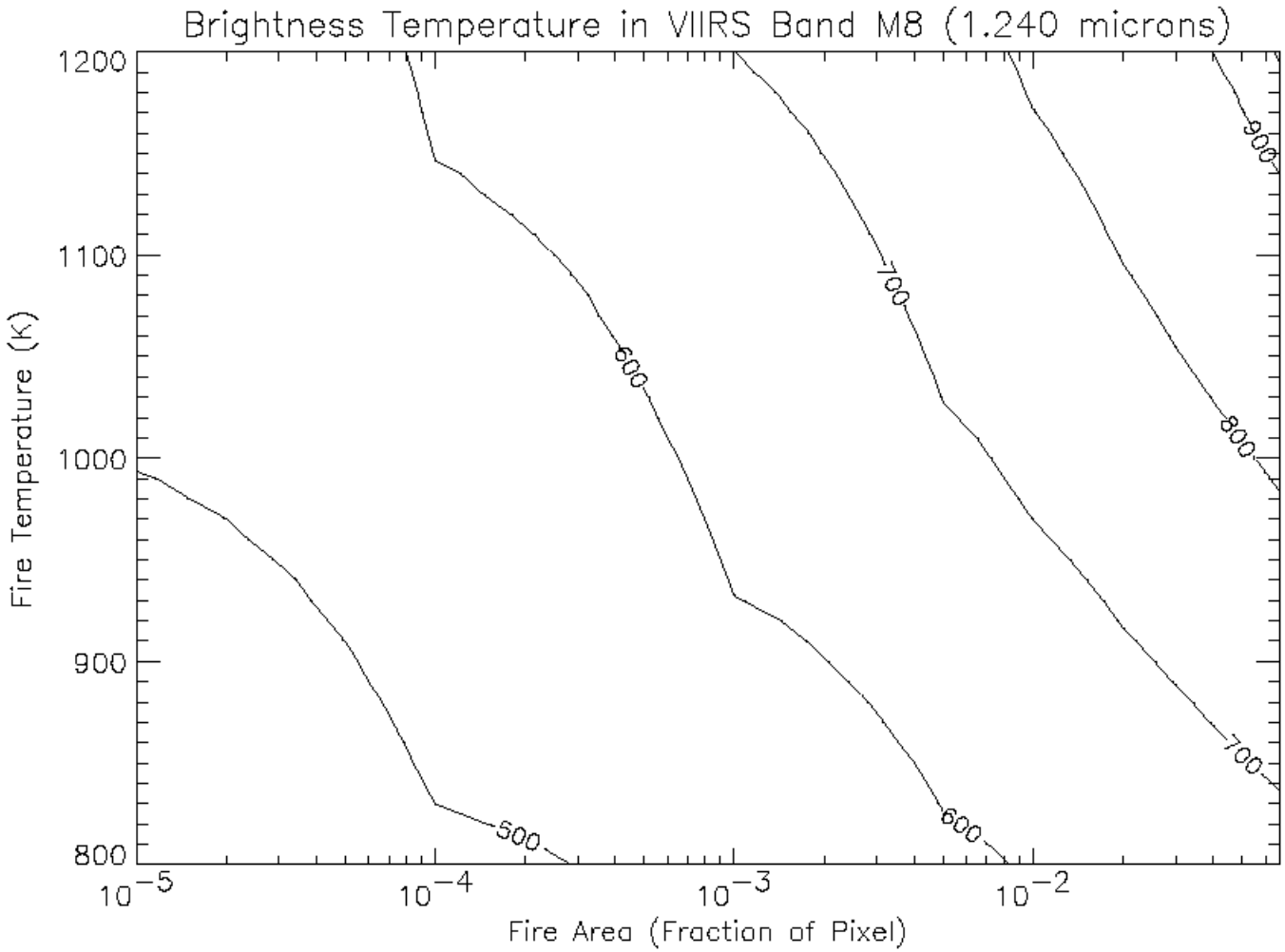

Figure 15. Active fires response of VIIRS band M8.

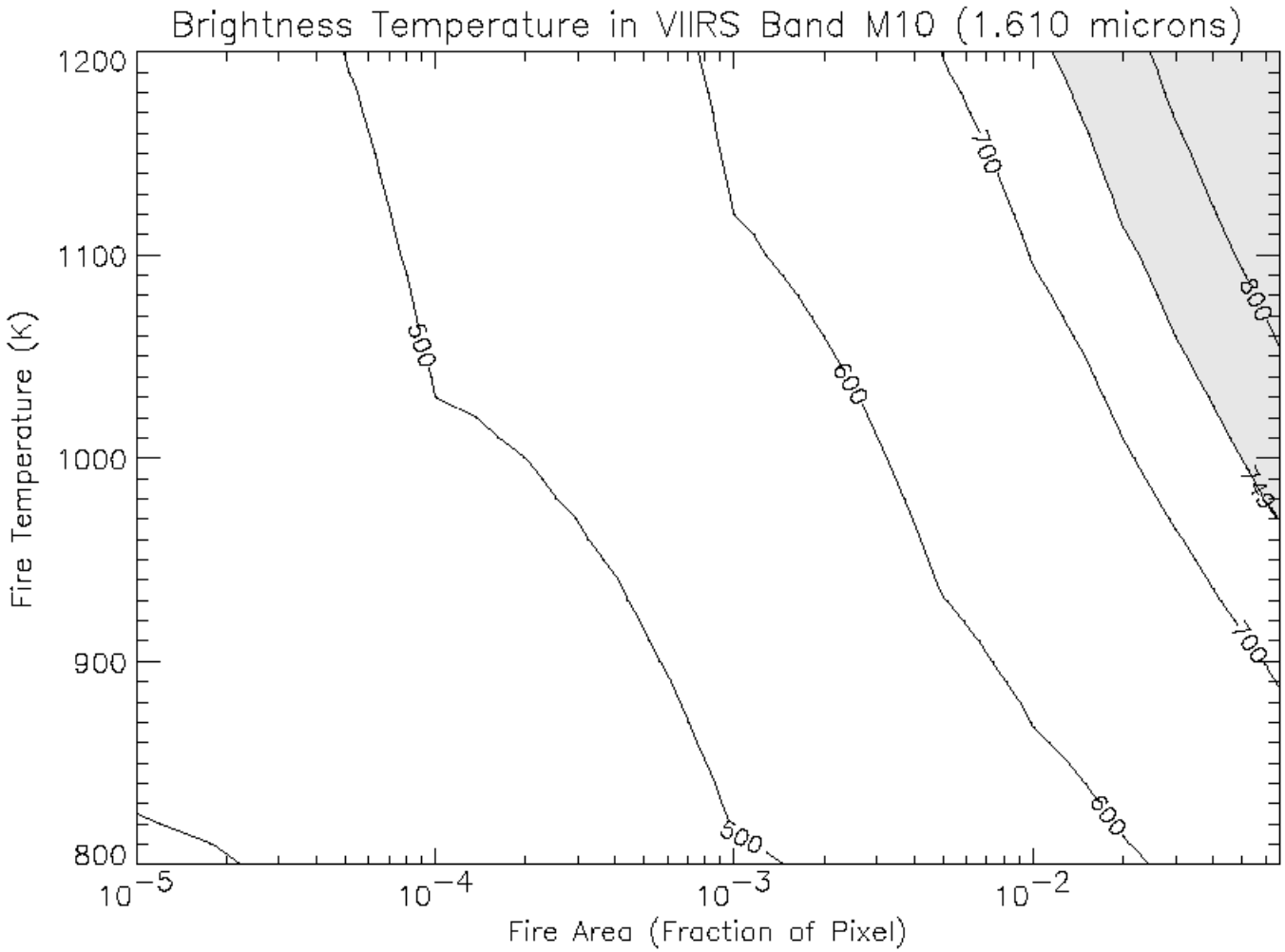

Figure 16. Active fires response of VIIRS band M10.

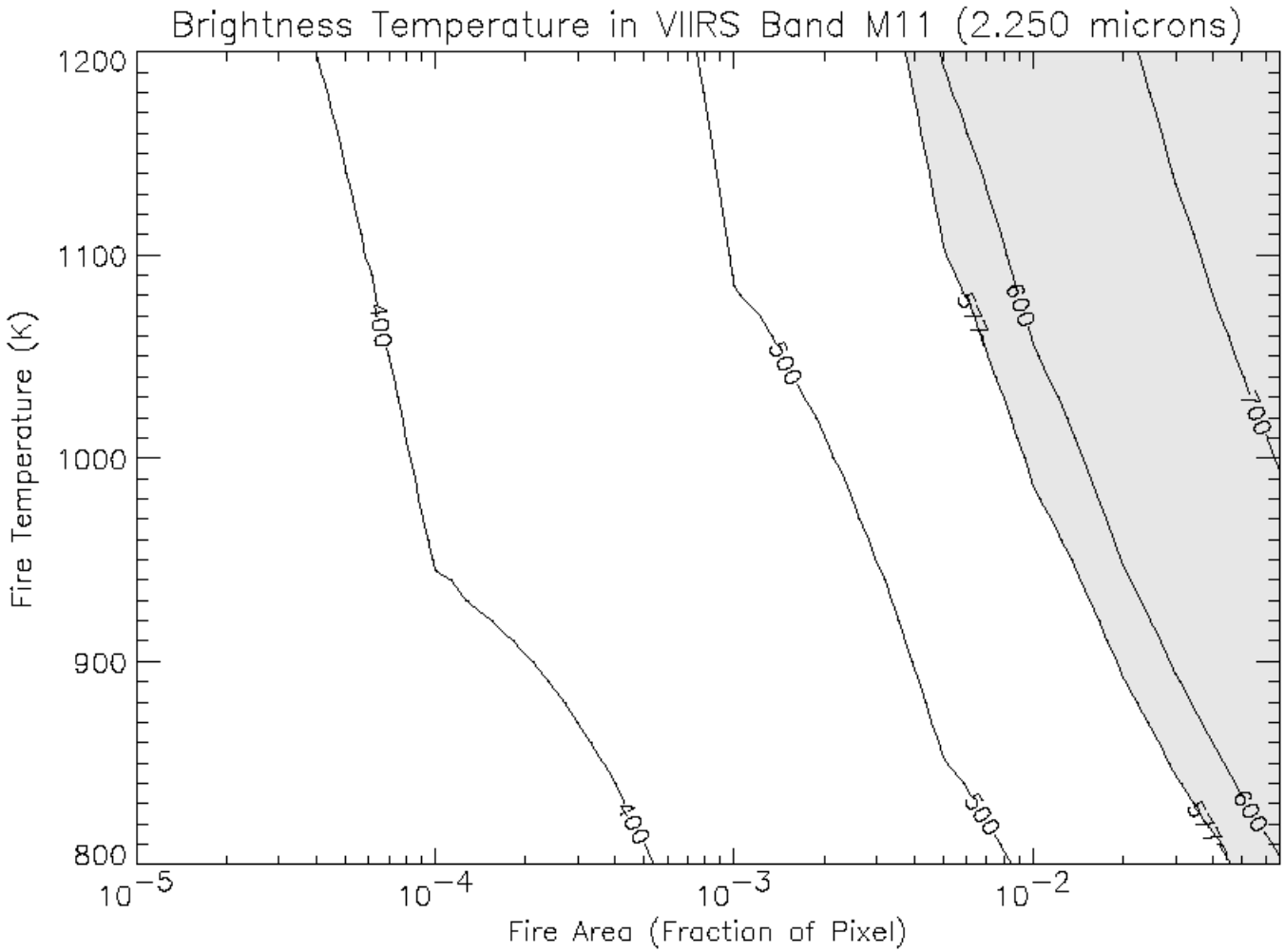

Figure 17. Active fires response of VIIRS band M11.

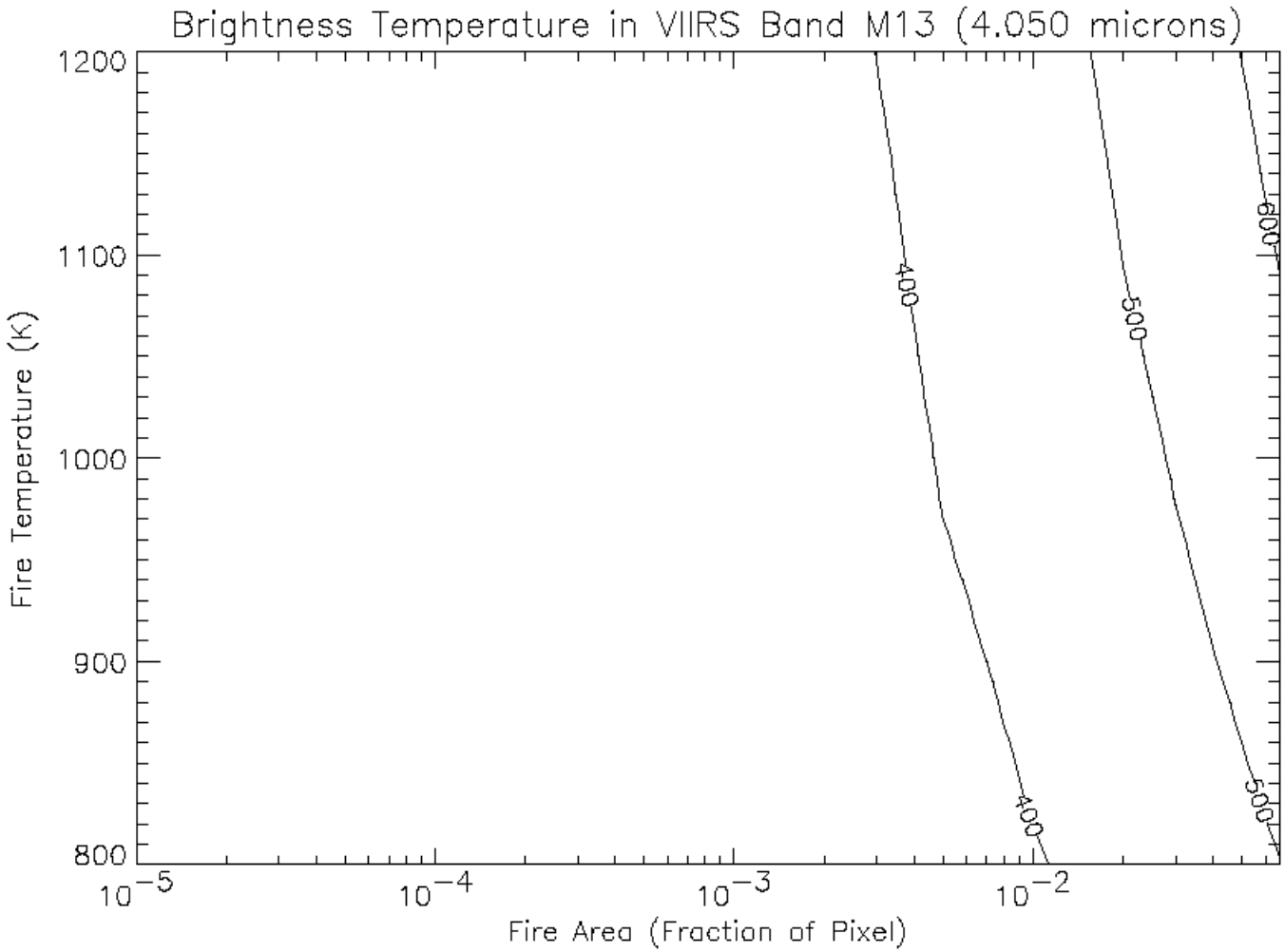

Figure 18. Active fires response of VIIRS band M13.

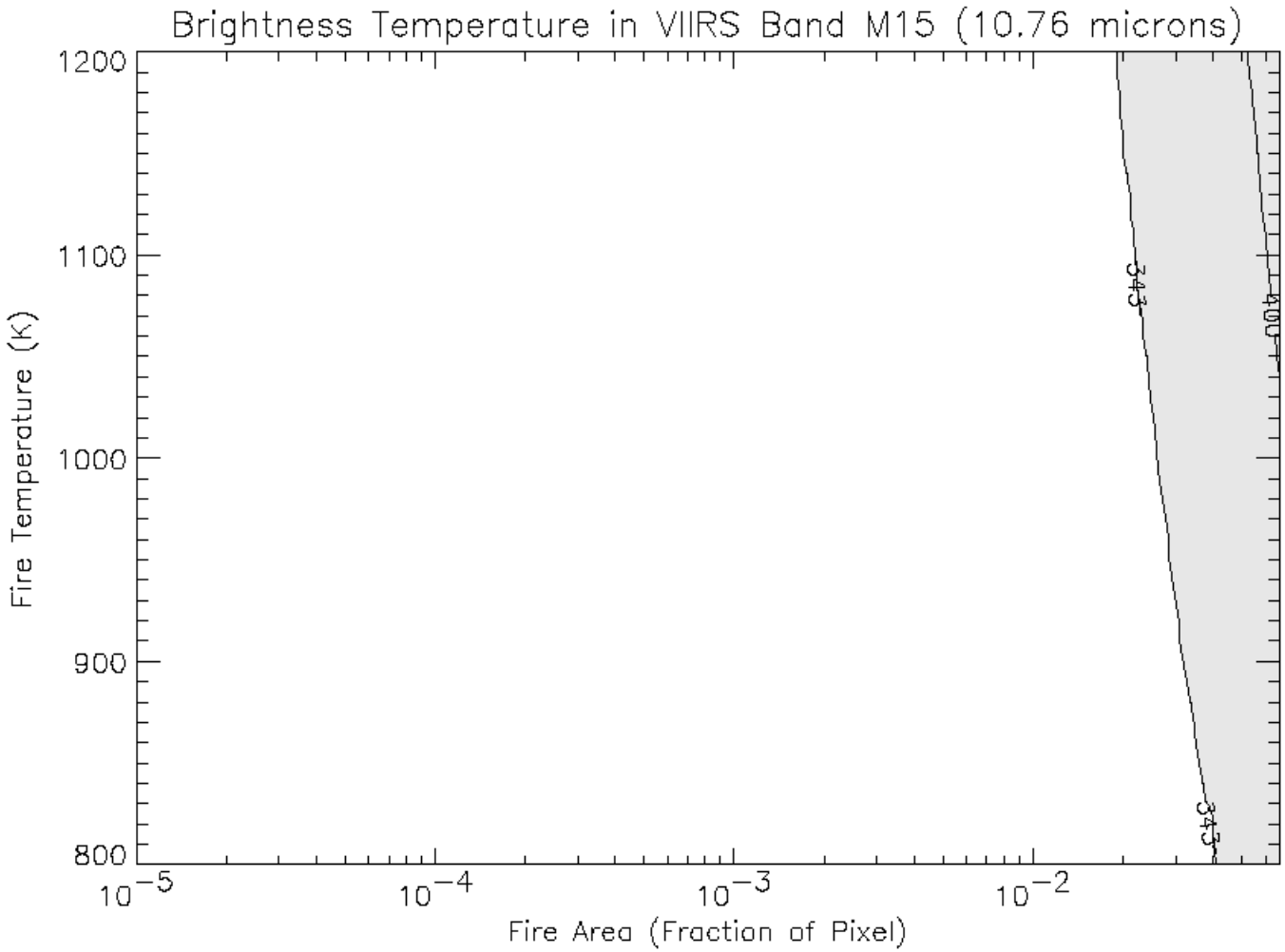

Figure 19. Active fires response of VIIRS band M15.

The VIIRS SRD categorizes the Active Fires Application as "Category IIB." The "II" indicates that the threshold requirements are allowed to drive the VIIRS design, balanced against cost, so long as the manifestation of these requirements does not endanger the quality of the Category I EDRs, namely Sea Surface Temperature (SST) and Imagery. The "B" indicates that the objective requirements should not be allowed to drive the design in any significant way. Most of the Category II VIIRS EDRs are Category IIA, which essentially places them somewhat higher in priority than Active Fires when trades are evaluated.

These prioritizations have led to the current, optimized VIIRS design, which provides the best value among over two dozen EDRs, but must do so at the expense of some EDR-specific specialization in the hardware, particularly when SST or Imagery is traded against another product. Since both SST and Imagery utilize the VIIRS LWIR bands, none of these bands can be driven high enough to provide coverage of the entire fire temperature/area measurement range. The best that can be done is M15, summarized in Figure 19. Clearly, this band saturates for over half of the temperature/area measurement range, and therefore cannot be utilized for quantitative retrievals of temperature and area in all cases. Increasing the saturation temperature in M15 would cause the quantization to noise ratio (QNR) to become larger than 1, which has already proven to be a problem for the SST community with regard to the MODIS Protoflight Model (PFM), as that 11 µm band has a saturation temperature of 400 K because of the MODIS fire requirements. The MODIS Flight Model 1 (FM1), to be carried on Aqua, has a much lower saturation temperature for this reason, and the same has been done for the VIIRS design. The thermal imagery band on VIIRS—I5—is a key band for the Imagery EDR, and therefore also does not possess enough flexibility to solve this dilemma.

Two important points must be made regarding the above discussion. First, there is still a possibility that dual gain could be implemented in later models of the VIIRS, which would allow M15 to reach the necessary saturation temperature. Second, even though the present band M15 would saturate over half the measurement range, this is not equivalent to saturation over half of all active fires. In fact, there have been some indications in non-published research that well over 90% of the active fires on Earth would leave M15 unsaturated. On the other hand, it is often the largest/hottest fires that are of the most interest to the user community. Further progress must be made in arriving at the optimum solution for retrieval of this product, however the VIIRS product even now is expected to provide a wealth of new information about the behavior of fires and the associated carbon exchange and transport.

To address regimes where M15 does presently saturate, the VIIRS Active Fires algorithm must provide a data processing solution. The approach adopted late in Phase I algorithm development was to activate several NIR/SWIR bands at night, so that these bands could be used together with M13—which has been designed to cover the full fire temperature/area measurement range—in instances where M15 saturates, both day and night. More detail on this approach is provided in Section 3.3.2.3. Recent work at NASA and SSAI has suggested that this technique causes errors and discontinuities at the switch points that are not tolerable within the error specifications for Active Fires, hence our continued search for alternative solutions.

3.3.1.2 Historical Development of Fire Products

Matson and Dozier (1981) showed that simultaneous use of the 3.8 μm and 11 μm channels provides the capability to detect high temperature sources such as steel plants and waste gas flares, with the 3.8 μm channel particularly sensitive to such targets. Matson *et al*. (1984) determined that one can utilize the temperature difference between the two bands to calculate the area and temperature of a hot target. This alone does not guarantee that a fire has been detected, but the transient nature of fires can be used to screen out industrial areas, as the latter subsist from one snapshot of a given location to the next.

In an effort to begin characterizing the background environment surrounding a fire, Matson and Holben (1987) investigated the use of the Normalized Difference Vegetation Index (NDVI) in addition to the MWIR-LWIR temperature difference, and they found it to show good promise for burn scar detection and other similar phenomena.

One of the challenges facing the early development of fire detection techniques was the difficulty in applying any one algorithm globally. Until the past decade or so, most fire detection techniques were simple threshold tests with the brightness temperatures and brightness temperature differences in the available channels. This approach must be applied differently in forests than in savannas. The former tend to provide a relatively cooler environment for fires than the latter, and any threshold optimized for one scenario will fail somewhat for the other. In an attempt to surmount this problem, Franca *et al*. (1995) developed a multispectral methodology based on NOAA-11 AVHRR data, to at least partially resolve the numerous problems with error sources such as large surface heterogeneity, clouds, smoke, haze, background emissivities, and so forth. Their technique obtained more realistic results, and did not overestimate or underestimate the number of fires sensible by the satellite. This particular algorithm seems to work fairly well in both savanna and forest environments. It starts with the identification of candidate pixels using the channel 3 (3.7 μm) threshold of saturation, around 320 K. Vickos (1991) showed when there is no ambiguity between fire and its environment, this test alone is sufficient. The Franca algorithm subsequently computes the brightness temperature difference between channels 3 and 4, ΔT_{34}, to check for cloud effects. A second difference between AVHRR channels 4 and 5, ΔT_{45}, is applied to account for additional cloud effects. ΔT_{34} tends to provide better separation of fires, whereas ΔT_{45} allows fairly robust separation of fires from clouds.

Harris (1996) derived a different approach, helping to signal a new paradigm for active fire detection. Rather than applying straight thresholds, the algorithm attempts to develop a context for the candidate pixel in question. The algorithm is applied to an image of ΔT_{34}. First, it calculates the difference between the center pixel and its immediate background, $\Delta(\Delta T_{34})$. The immediate background is defined by centering a 3x3 pixel window on the target pixel and taking the mean of ΔT_{34} for the eight surrounding pixels. $\Delta(\Delta T_{34})$ is then compared with the subimage natural variation, which is defined as the maximum $\Delta(\Delta T_{34})$ for a fire-free portion of the subimage. This fire-free portion is in turn defined by a fire-screened 45x45 km area taken from top NE corner of the subimage. Fire screening is conducted by rejecting pixels detached from the natural variation frequency distribution tail. If $\Delta(\Delta T_{34})$ is greater than the natural variation, the

pixel is flagged. About 22% false alarms were found with this approach, caused primarily by industrial sources or clouds.

The transition to contextual fire detection was completed with Flasse and Ceccato (1996). Placed in contrast with threshold techniques, their algorithm uses pixels in the immediate neighborhood to derive a localized context for fire detection that is self-adaptive and consistent over large areas and through different seasons. The algorithm has been successfully tested in most areas of world. It works well because it is relative instead of absolute in nature, so that hot savanna fires can be detected just as robustly as cooler forest fires without adjusting thresholds. There are two stages to the algorithm: selecting candidate pixels (potential fires, PFs), and then confirming or rejecting the pixel based on the behavior of its immediate neighbors. A pixel is selected as a PF if $T_3 > 311$ K and $\Delta T_{34} > 8$ K. The low threshold for the first test is set to avoid rejection of cooler fires. A second test eliminates pixels where the reflectance in the near IR channel, ρ_2, is greater than or equal to 20%. This allows some screening of sunglint, bright soil, and clouds.

The second stage of the Flasse and Ceccato algorithm works as follows. For each PF, statistics are calculated for a variable sized context window (from 3x3 up to 15x15 pixels) around the PF. The size of the window hinges upon having at least 25% of the neighboring pixels as background, and at least three pixels must be eligible for the computation. If these conditions are not met, the PF is rejected. Otherwise, the following quantities are computed:

- T_{3b}, the mean of the channel 3 brightness temperature T_3 for the fire background
- σ_{T3b}, the standard deviation of the channel 3 brightness temperature for the fire background
- T_{34b}, the mean of the difference between the channel 3 and channel 4 brightness temperatures, T_3 and T_4 for the background
- σ_{T34b}, the standard deviation of the difference between the channel 3 and channel 4 brightness temperatures for the background

Finally, the contextual test is applied. A PF is confirmed to be a fire when

$$T_{3PF} - (T_{3b} + 2\sigma_{T3b}) > 3 \text{ K}$$

and

$$T_{34PF} > T_{34b} + 2\sigma_{T34b}$$

The success of contextual fire detection methods in recent years has led to the adoption of the methodology for the MODIS Fire Products, described in Kaufman and Justice (1998). Briefly, the MODIS fire detection algorithm works as follows:

1) Cloud detection and scan angle. The MODIS cloud mask and a 45 degree scan angle cutoff are used to disqualify pixels for subsequent processing.

2) Atmospheric correction. The brightness temperatures in the 4 μm and 11 μm bands, T_4 and T_{11}, respectively, are corrected for gaseous absorption.

3) Background characterization. This follows Flasse and Ceccato (1996), only it allows the window to be sized as large as 21x21 pixels. Energetic fire pixels are eliminated from analysis if $T_{41} = T_4 - T_{11} \geq 20$ K (10 K at night) and $T_4 > 320$ K (315 K at night). If these tests are passed, then the statistical parameters T_{11b}, δT_{11}, T_{4b}, δT_4, T_{41b} and δT_{41} are calculated, where the subscript b denotes a mean and the prefix δ denotes a standard deviation.

4) Fire detection. If $T_4 < 315$ K (305 K night) or $T_{41} < 5$K (3K at night), the pixel is rejected. If δT_4 and δT_{41} are less than 2K, they are set to 2K. The pixel is defined to contain an active fire if the following conditions are met:

   $\{[(T_4 > T_{4b} + 4\delta T_4)$ or $T_4 > 320$ K (315K at night)] and

   $[(T_{41} > T_{41b} + 4\delta\Delta T_{41})$ or $T_{41} > 20$ K (10K at night)]}

   or $\{T_4 > 360$ K (330 K at night) }

5) Glint exclusion. A fire pixel is excluded during the day if the reflectance in the red band, $\rho_{0.64}$, is greater than 0.3 and the reflectance in the near IR band, $\rho_{0.86}$, is greater than 0.3, and the glint angle is less than 40 degrees. This is the end of MODIS Level 2 processing for fires. Further processing is MODIS-specific and targets the emitted energy, as well as identification of the smoldering/flaming stage.

Raytheon has established some heritage with fire detection recently as part of efforts with the Hazard Support System (HSS). Raytheon (1998) summarizes the trades that went into the selection of fire detection algorithms for the HSS. These trades are summarized in Table 10.

Because of its clear advantages over older threshold techniques, the contextual analysis approach was adopted by Raytheon for the HSS. Two algorithms were selected, one based on Prins and Menzel (1992), Flasse and Ceccato (1996), and reported in Justice and Dowty (1993), and the other based on a similar approach developed at NASA/GSFC for use with AVHRR 1 km data. The primary algorithm proceeds in the following sequence:

1) Geolocation

2) Calibration

3) Cloud masking (using Saunders and Kriebel (1988) for AVHRR, Prins and Menzel [1996b] for GOES)

4) Threshold fire test

5) Sunglint rejection

6) Contextual fire detection

For the threshold fire test, it was recommended that values be defined by month, and that a weekly NDVI product be incorporated for background characterization. The sunglint rejection uses red and near IR reflectances, much in the same manner as for MODIS. The contextual fire detection uses windows ranging in size from 3x3 to 15x15 pixels.

Table 4. Algorithm trades conducted by Raytheon for the Hazard Support System (HSS).

Author of Algorithm (Year)	Type	Reported Performance
Matson and Dozier (1981)	Fixed threshold	Detection of steel mills and oil field gas flares. Wildfire detection not part of experiment.
Flannigan and Vonder Haar (1986)	Fixed threshold	AVHRR fire detection success: 80% not obstructed by cloud or smoke. Fires under 10 acres detected 12-14% of the time.
Kaufman *et al*. (1990)	Fixed threshold	AVHRR false positives: 10% (Melinotte and Arino, 1995)
Setzer and Pereira (1991)	Fixed threshold	AVHRR fire detection success: 96% of detected fires were verified and no reports of missing fires.
Lee and Tag (1990)	Lee and Tag	Unknown
Prins and Menzel (1992)	Spatial analysis	Unknown
Justice and Dowty (1993)	Spatial analysis	AVHRR fire detection success: 37.5% (Elvidge *et al*. 1997)
Flasse and Ceccato (1996)	Spatial analysis	AVHRR false positives: 15% (Flasse and Ceccato, 1996). AVHRR fire detection success: 37.5% (Elvidge *et al*. 1997)
Prins *et al*. (1996a)	Spatial analysis	GOES 8 fire detection success: 22.2% (Elvidge *et al*. 1997). Minimum size fire detected: 10 acres.

3.3.2 Mathematical Description of VIIRS Approach

3.3.2.1 Fire Detection

The baseline VIIRS fire detection algorithm is an extension of the MODIS contextual analysis heritage. It proceeds as follows:

1) *Saturation Handling*. All of the steps following this one assume as input two unsaturated signals, one in band M13, and the other in either band M15 or one of the relevant NIR/SWIR bands (M7, M8, and M10). For fires that do not saturate M15, the baseline pair for fire detection and temperature/area measurement is M13 and M15. For fires that do saturate M15, fire detection will likely continue to proceed with this baseline pair, setting M15 equal to its saturation value for the purposes of the threshold and contextual

tests. For fire temperature and area measurement, when M15 saturates, the algorithm may switch to NIR and/or SWIR data to accompany M13. When M13 saturates, fire temperature and area retrieval will not be executed. For a thorough discussion of VIIRS band saturation and our strategy for addressing Active Fires when this saturation occurs, the reader should consult section 3.3.2.3.

2) *Calibration and Geolocation*. The VIIRS Build SDR Module generates the VIIRS 750-m Earth View SDR, which includes TOA brightness temperatures for all bands relevant to Active Fires. This SDR also includes appended geolocation and solar/viewing geometry information for each pixel. We thus have the TOA brightness temperatures in bands M13 and M15—T_{13}^* and T_{15}^*, respectively. If either band is saturated, the corresponding TOA brightness temperature is set to the saturation brightness temperatures in that band.

3) *Surface Type, Cloud, and Sunglint Masking*. If the Quarterly Surface Types IP indicates the pixel is water, permanent snow/ice, or urban, processing ceases. The VIIRS Cloud Mask IP is checked for the presence of cloud or sunglint. If the relevant individual tests categorized the pixel as definitely clear, processing continues to Step 4. If the relevant individual tests categorized the pixel as definitely cloudy and not thin cirrus, processing ceases, and all Active Fires fields are filled with predefined "missing" values. If the relevant individual test categorized the pixel as probably clear or probably cloudy, processing continues, and the Land Quality Flag (LQF) output will indicate possible obscuration by cloud. The performance specification is not guaranteed in that case. If the relevant individual tests categorized the pixel as contaminated by correctable thin cirrus, a thin cirrus correction will be applied to generate new values of T_{13}^* and T_{15}^*, and processing continues, with the pixel flagged by the LQF output, and the performance specification is not guaranteed. If the Cloud Mask categorizes the pixel as contaminated by sunglint, processing ceases. Note that even if a pixel has passed the Cloud Mask testing, we apply some additional tests below that further ensure the minimization of cloud contamination and/or false fire detections.

4) *Atmospheric Correction*. NCEP column water vapor is used to correct T_{13}^* and T_{15}^* to surface brightness temperatures T_{13} and T_{15}. This is also the step where aerosol corrections using the VIIRS Aerosol Optical Thickness and Aerosol Model Information IPs would be applied. The exact form of these corrections is still TBD. The VIIRS Precipitable Water EDR is not used as an input here because it relies on the MWIR and LWIR bands for retrievals, and these retrievals will be questionable for pixels with active fires.

5) *Identification of Potential Fires*. Let $\Delta_{35} = T_{13} - T_{15}$. If $T_{13} < T_{min}$ or $\Delta_{35} < \Delta_{min}$, then the pixel is rejected. Otherwise, the pixel potentially contains a fire and processing continues. The baselines for T_{min} and Δ_{min} are yet to be determined; the MODIS values cannot be assumed as starting points, because the VIIRS bands have different spectral and spatial characteristics.

6) *Near Infrared (NIR) Reflectance Test*. Borrowing from the work of Li et al. (2000), we have introduced a NIR reflectance test to reduce commission errors (discussed further in section 3.4.4). Applied to only the pixel in question, the test rejects the pixel if the M7

reflectance $R_{nir} > R_{max}$ (set to 22% in Li et al., 2000). This test is only applied during the daytime, although it could be applied at night with little harm beyond unnecessary computation time.

7) *Background Characterization*. A WxW pixel window is generated around the pixel in an attempt to construct a background characterization. This window may range from W_{min}xW_{min} up to W_{max}xW_{max} pixels in size. The current baselines for W_{min} and W_{max} are 3 and 21, respectively. At least f_{min} of the neighboring pixels must qualify as background, where f_{min} is in percent. At least N_{min} of the neighboring pixels must qualify as background. The current baselines for f_{min} and N_{min} are 25% and 3, respectively. A pixel qualifies as background if it is not a potential fire pixel (using the criteria of Step 4), is not contaminated by cloud (as defined in Step 2; thin cirrus and atmospheric corrections are also applied to background pixels), and is of the same surface type as the central pixel under consideration (information supplied by the Quarterly Surface Types IP). For any pixel in which either band is saturated, the corresponding brightness temperature is set to the saturation temperature for that band. If the f_{min} and N_{min} criteria cannot be met, the pixel is rejected. If the f_{min} and N_{min} criteria are met, the following statistical quantities are computed for all background pixels: the mean brightness temperatures in M13 and M15, denoted by μ_{13} and μ_{15}, respectively; the standard deviations in the brightness temperatures in M13 and M15, denoted by σ_{13} and σ_{15}, respectively; the mean difference between the brightness temperatures in M13 and M15 ($T_{13} - T_{15}$), denoted by μ_{35}; and the standard deviation of the difference between the brightness temperatures in M13 and M15, denoted by σ_{35}.

8) *Fire Detection*. The pixel is defined to contain an active fire if one of the following two conditions applies:

   a. $[(T_{13} > \mu_{13} + 4\sigma_{13})$ or $(T_{13} > T_{crit})]$ and $[(\Delta_{35} > \mu_{35} + 4\sigma_{35})$ or $(\Delta_{35} > \Delta_{crit})]$

   b. $T_{13} > T_{abs}$

The quantities T_{crit}, Δ_{crit}, and T_{abs} are still to be determined (TBD) during the course of VIIRS algorithm development.

3.3.2.2 Subpixel Average Fire Temperature and Subpixel Fire Area

Once a pixel has been categorized as containing an active fire by the technique summarized in Section 3.3.2.1, computation of subpixel average fire temperature and subpixel fire area commences. The technique for computing subpixel fire temperature and area is an extension of that introduced by Dozier (1981), using modifications suggested by Giglio and Kendall (2000).

The spectral radiance at the top of the atmosphere can be approximately represented as:

$$\begin{aligned} R_\lambda &= f\left[\varepsilon_\lambda \tau_\lambda B_\lambda(T_{fire}) + path_R_\lambda\right] + (1-f)\left[\varepsilon_\lambda \tau_\lambda B_\lambda(T_{bg}) + path_R_\lambda\right] \\ &= \varepsilon_\lambda \tau_\lambda \left[f B_\lambda(T_{fire}) + (1-f) B_\lambda(T_{bg})\right] + path_R_\lambda \end{aligned} \tag{1}$$

where

f : fraction of pixel covered by fire;

ε_λ : surface emissivity at the wavelength λ;

τ_λ : atmospheric transmittance at the wavelength λ from the surface to the top of the atmosphere;

B_λ : Planck function at the wavelength λ;

T_{fire} : the temperature of the active fire;

T_{bg} : the surface temperature of the background ;

$path_R_\lambda$: path radiance, contributed by the atmosphere.

Theoretically, two equations formed by satellite measurements for two bands located at 4.05 µm and 10.76 µm can facilitate the measurement of subpixel fire area and temperature, so long as we borrow information from neighboring pixels for the characterization of the background. In order to do so, we must reduce the number of unknowns in (1) to two, yielding a system of two equations that can be solved for two unknowns. In the strictest sense, (1) abounds with unknowns. The fire fraction f, the spectral emissivity ε_λ, the atmospheric transmittance τ_λ, the fire temperature T_{fire}, the background temperature T_{bg}, and the path radiance $path_R_\lambda$ are all unknown parameters. The key is to make several assumptions, combined with the attempted retrieval of the remaining parameters not fully addressed by the assumptions.

The two parameters being sought are f and T_{fire}. These are therefore assumed to remain unknown in the simplification of (1). A hidden assumption in (1) is that spectral emissivity ε_λ is the same for both the fire and the background. A fire with sufficient path length through the flames will indeed behave much like a blackbody, and in the LWIR most surfaces have an emissivity very close to 1. But in the MWIR, some surfaces depart substantially from blackbody behavior, as seen in Figure 10. Most prominent is the behavior of soil. This has significant implications for brush or agricultural fires, where a substantial soil signal is present in the weighted surface emissivity. In an attempt to account for the variability of emissivity, the VIIRS algorithm will incorporate the Surface Type EDR to allow a refinement of the emissivity estimate for M13 and M15. This essentially converts ε_λ into a known parameter, albeit with some level of error. Estimates of this error will be derived in future sensitivity studies.

The primary gases affecting τ_λ are water vapor and carbon dioxide. Water vapor is by far the more important of these two gases, having a substantial effect on the radiances in both M13 and M15. Carbon dioxide primarily affects M13, but the degree to which this alters the TOA radiances has not yet been comprehensively measured in the VIIRS algorithm development effort. If further sensitivity studies indicate a strong dependence on column CO2, which of course will be more volatile in regions associated with biomass burning, an attempt may be made to incorporate a corresponding input into the VIIRS fire temperature/area measurement algorithm. For the present, water vapor is considered the only significant parameter. This

information will be incorporated via the operational NCEP analyses. These data will be used to determine τ_λ and convert it into another known parameter, with some associated level of error in the measurement.

Path radiance is caused by two principal effects: atmospheric scattering of downwelling and upwelling radiation, and atmospheric emission. An assumption is made for the VIIRS algorithm that neither of these is significant compared to the dominant signal in the MWIR or LWIR. In the LWIR, the background signal is expected to be much larger than the path radiance. In the MWIR, the fire signal is expected to be much larger than the path radiance. Complications arise when the LWIR saturates, and the algorithm must switch to the SWIR. This and other issues with using SWIR data will be discussed in Section 3.3.2.3. When the LWIR signal is unsaturated, however, the path radiance is considered negligible and is therefore ignored.

This leaves three unknowns in the system of equations represented by (1): f, T_{fire}, and T_{bg}. Following Dozier (1981), we assume that T_{bg} can be determined from surrounding, non-fire pixels. The VIIRS Quarterly Surface Types IP will allow us to use only surrounding pixels with the same surface type as the central pixel for retrieving T_{bg}. This will allow for substantial reduction in the errors associated with T_{bg}, some of which are discussed in Giglio and Kendall (2000). The result is an set of two equations with two unknowns—f and B_{fire}, the latter of which can be converted to T_{fire} under the assumption of unity emissivity. A number of different numerical approaches can be used to solve these equations, such as those presented in Press et al. (1989).

3.3.2.3 Saturation Handling

As is clear from Figure 19, a significant portion of the fire temperature/area measurement range will saturate band M15. In these instances, fire detection is still viable, but temperature and area measurement become much more difficult. As was discussed in Section 3.3.1.1, it was not possible to mitigate this problem within the best-value system optimization solution for VIIRS. The burden therefore falls upon the algorithm to circumvent the saturation of M15 and still deliver estimates of fire temperature and area.

It is worthwhile to cover the different options that were considered for the handling of saturation, as the results of the trades may serve as guidance for the development of future remote sensing systems that must retrieve fires in addition to other products. In all, five separate solutions were considered; two remain as ground processing options, but neither is low enough in risk to fully address the problem. In brief, the five options considered were:

1) Increasing the saturation temperature in M15 (11 μm) from 343 K to 422 K. This would have been the most desirable course of action from the standpoint of fire temperature and area retrievals, because it would allow continuous use of the heritage Dozier technique throughout the measurement range. It was rejected because it caused the quantization to noise ratio at lower temperatures to be larger than 1, causing stair-step patterns in images of the Category I SST EDR.

2) Activating several shorter wavelength bands at night, so that when M15 saturates, the fire temperature/area retrieval algorithm can pivot around M13 (4 μm) and use the NIR or

SWIR bands in place of M15. This option still exists as our primary means of addressing fire temperature and area when M15 saturates, however it introduces errors and discontinuities that exceed the uncertainty requirements (Table 11).

3) Increasing the saturation temperature in I5 (11.45 μm at imagery resolution) to 678 K, matching the effective capability of M13. The much higher temperature would be necessary because of the higher spatial resolution and sharper imagery point spread function in I5 compared to the moderate resolution bands. This option was rejected because it caused unacceptable loss of margin at the present stage of the VIIRS program for a key band used by the Category I Imagery EDR.

4) Increasing the saturation temperature in M14 (8.55 μm) to 457 K, again matching the effective capability of M13. This is preferable to using NIR and/or SWIR bands when M15 saturates, because the signal in M14 behaves much like that in M15. Additionally, M14 is not directly used by any Category I EDRs. The change was rejected, however, because of uncertainties due to water vapor and combustion product absorption, and also because it may have negative impacts on cloud phase retrievals, which are a precursor to all of the VIIRS cloud algorithms.

5) Exploiting the behavior of VIIRS beyond the specified maximum temperature in a given band. Improving on the MODIS heritage, the VIIRS bands do not actually saturate at and beyond a given value; rather, they become nonlinear beyond the specified maximum radiance until they reach what would be a saturation point, and then the response "folds over" and begins to decrease with increasing temperature. For most VIIRS bands, this is an important new effect to be wary of in SDR processing, but for Active Fires, it might be of some benefit. The signals in the unaggregated detector footprints for M13 could be used to determine which detectors covered an active fire or fires, and then the signals in M14, M15, and M16 could be used to determine which side of the saturation point we are on. Assuming pre-launch characterization, the temperature in M15 could then be computed as used as normal, as illustrated in Figure 20. Unfortunately, this illustration shows a best-case scenario for Active Fires. In reality, the useful response beyond the specified maximum temperature in a band is limited by the digital number (DN) range, and any such performance beyond Tmax is margin that cannot be assumed prior to the fabrication of the instrument. Still, this approach may serve to provide a slight enhancement for any given VIIRS flight unit, and it remains under consideration toward that end.

Of all the options considered, only the NIR/SWIR fallback strategy remains, albeit at significant risk to the uncertainty requirements for fire temperature and area. Late in Phase I algorithm development, the algorithm team worked with the sensor team to implement a hardware solution that would facilitate this approach. Specifically, the sensor specification called for the activation of bands M7, M8, M10, and M11 both day and night. Let us now consider what occurs in these bands when band M15 saturates, moving from longer wavelengths to shorter ones.

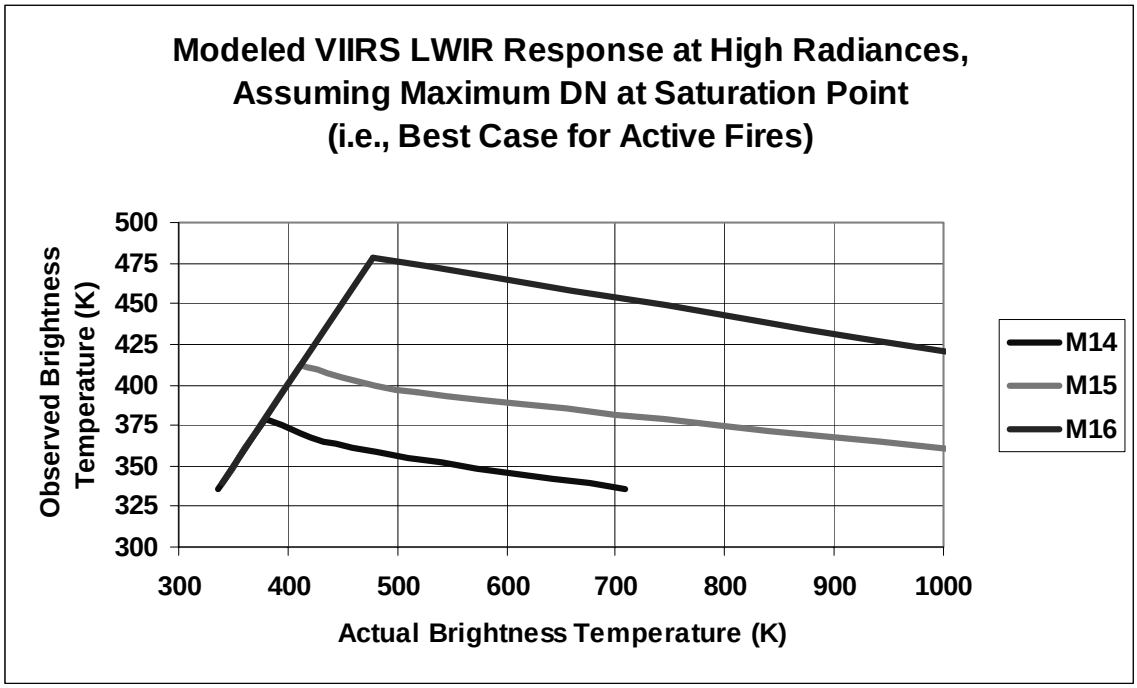

Figure 20. Idealized VIIRS band behavior beyond specified maximum temperature for fire temperature/area measurement (actual instrument performance will fall somewhere short of this illustration due to limitations of the realized DN range).

M15 saturates at a TOA brightness temperature of 343 K (Ignoring the 20% overhead applied in the sensor design process). From Figure 19, one can get a sense of what combinations of fire temperature and area cause this to happen, ignoring atmospheric attenuation. It is immediately apparent from Figure 17 that band M11 does not help much in this situation. As a result, the sensor specification has been modified to inactivate M11 at night. M13, on the other hand, has been specifically designed to cover the entire temperature/area measurement range. This was possible because of the tractability of dual gain in the SWIR/MWIR focal plane. Implementation of dual gain in the LWIR focal plane is much more difficult, however there may be an attempt to revisit this possibility for the second VIIRS flight model and/or beyond (effectively revisiting option 1 in the list above).

Now consider the data in Figure 16, for band M10 (1.61 µm). In this band, saturation occurs for larger fires than for M15, although for smaller fires with very high temperatures, saturation actually occurs earlier in M10. In these instances, one would switch to band M8 (1.24 µm), which covers almost the entire measurement range. The strategy would be to use M13 as a pivot point. For fires that do not saturate M15, M13 and M15 would be used in (1) to derive f and T_{fire}. For fires that saturate M15, M13 would become the longer-wavelength band in (1), and M10 would become the shorter-wavelength band, until M10 saturates. At that point, the algorithm would switch to M8. For the most extreme cases, M7 (865 nm) would be used.

There are three significant hurdles to overcome with this new approach to fire temperature and area measurement. First, the system of equations in (1) becomes more unstable when the LWIR is abandoned, because most of the information in both bands being considered originates in the

fire, and not in the background. This also introduces discontinuities in computed fire temperature and area between the M13/M15 regime and the M13/SWIR regime. Second, the scattering contributions to the path radiance become more significant the shorter the wavelength of the bands used in (1), causing the assumption that this term can be neglected to break down. Third, daytime retrievals will be contaminated by a solar reflective signal in the NIR and SWIR, and terminator orbit retrievals will be affected by a solar reflectance contribution that, while small, is significantly more difficult to pin down. If these three problems can be overcome algorithmically, the NIR/SWIR mitigation strategy for saturation in the LWIR should yield very useful measurements of f and T_{fire}. Whether these measurements are of sufficient quality to meet the EDR specifications remains to be proven.

To address the issue of mathematical instability in the system of equations represented by (1), it may be worthwhile to incorporate more than two bands into the calculation. Following Phase II adjustments, both M7 and M8 now cover the entire fire/temperature area measurement range without saturation. This would allow the simultaneous usage of M7, M8, and M13 in (1) whenever M15 saturates. Whether this adds sufficient stability to the calculations is unclear, but it might also allow for better handling of path radiance.

To mitigate the increased effects of scattering in the SWIR and NIR, a climatological aerosol optical thickness correction might prove quite useful. During the day, the VIIRS Aerosol Optical Thickness EDR will be based in part on the radiance contaminated by the fire, rendering it unreliable as a correction source. At night, a direct measurement of optical thickness is not available. Persistence from the daytime measurements of aerosols might prove more robust than a climatology. Neither approach, however, will account for aerosols associated with the burning itself.

To mitigate the effects of the solar reflective signal, the Gridded Monthly Mean Reflectance IP will be utilized, in combination with the solar/viewing geometry for the pixel in question. The errors inherent in this process have not yet been explored.

Even with all these steps taken to reduce the overall risk in the NIR/SWIR fallback approach, recent sensitivity studies have indicated that the discontinuities when switching from M13/M15 to M13/M10, for example, are larger than the total error allotment for fire temperature. These discontinuities are due to a more pressing problem, which is that the answer derived from the NIR/SWIR bands is generally going to be wrong, as it has insufficient sensitivity to the background or to the smoldering portion of a fire. Continued development must be performed to determine if there is some means of rectifying this situation, however a suitable alternative approach has not yet been derived.

3.3.2.4 Burn Scar Detection

The detection of burn scars is another extremely valuable mechanism for determining the exchange of carbon from the surface into the atmosphere. Examples of recent progress on burnt area measurement can be found in Martin and Chuvieco (1993), Pereira and Setzer (1993), Kasischke and French (1995), Fernandez et al. (1997), Pozo et al. (1997), Barbosa et al. (1997), Eva and Lambin (1998), and Roy et al. (1999). The value of burn scar detection becomes starker when the saturation issues in the VIIRS LWIR bands are taken into account. Consequently,

Raytheon has added another baseline parameter to the Active Fires output—a burn scar detection flag. The spectral data and EDR products needed for this activity are already available in the VIIRS system, e.g., in the Vegetation Index and Surface Type EDRs and the large number of spectral bands in the reflected solar wavelengths, so it has no impact on the sensor design and only minimal impact on algorithmic and software development efforts. The long-term benefit is deemed sufficient to warrant the expenditure of these efforts, at least to first order, so that further integration into operational processing is not at risk.

At the present, due to schedule constraints in the delivery of the VIIRS prototype software, our efforts have focused on building an infrastructure for burn scar detection that can be filled in with specifics at a later date. The basic approach is briefly described here.

The signature of a burn scar depends rather dramatically on the type of vegetation that was burned. Depending on the type and the wavelength, the post-fire reflectance may be higher or lower than the corresponding pre-fire value. When some knowledge of the type exists, however, the spectral signature of a burn scar becomes more tractable, particularly in the case where a large amount of spectral information is available. This is precisely the case for VIIRS; every three months, the VIIRS ground system will produce a new global 1-km classification of the Earth's surface, recorded in the VIIRS Quarterly Surface Types IP that is already planned as an input to the Active Fires software unit. Additionally, VIIRS has an excellent array of spectral channels distributed across the visible, near infrared (NIR), short wave infrared (SWIR), middle wave infrared (MWIR), and long wave infrared (LWIR) wavelengths, as seen in Figures 8 through 11. This combination of inputs seems to lend itself to a very basic decision tree approach, much like that used for the production of the Quarterly Surface Types IP itself (summarized in *[Y2402]*). The VIIRS burn scar detection algorithm will therefore proceed as follows: for any land pixel that has failed the fire detection tests, the Quarterly Surface Types IP will be used to determine if burn scar detection makes sense, i.e., if the surface is not water or permanent snow/ice. The surface type is then used to determine a set of tests in the visible, NIR, SWIR, MWIR, and LWIR that establish with high confidence whether a burn scar exists. For example, if the pixel in question is classified as savanna, the visible signal is expected to have dropped below its normal value for savanna, while the NIR signal should be higher, the SWIR lower, the MWIR slightly higher, and the LWIR higher (although this last condition is the most temporary). Additionally, changes in NDVI that are not expected from seasonal norms will signal possible burnt areas.

Testing on regional datasets such as SAFARI 2000 will allow this decision tree approach to be refined for each major vegetation type. This should be a central task associated with Active Fires development efforts toward the launch of NPP. The initial software design is presented in *[Y3283]*.

3.4 ALGORITHM SENSITIVITY STUDIES

Because of the late arrival of the Active Fires product into the VIIRS requirements, and also because of its relative prioritization against other VIIRS EDRs, detailed sensitivity studies have not been possible to date. This activity must draw heavily upon the MODIS validation and verification infrastructure, to allow for a low-risk, low-cost system solution to be developed for VIIRS. Some information can be gleaned from simulations, however the behavior of real fires is

difficult to emulate in an artificial environment. Sensitivity studies should be targeted toward the error sources identified and described in the following subsections. The last subsection illustrates a sample application of several fire detection algorithm candidates to a single case study, however this did not include a thorough analysis of individual error sources, and does not apply on a global scale.

3.4.1 EDR Requirements

Table 5 lists the requirements specified by the Integrated Program Office (IPO) for the Active Fires product. The threshold requirements have been adopted as the VIIRS system specification for Active Fires. The meeting of these specifications is carried as a moderate risk at this writing, due primarily to the saturation issues discussed earlier in this document. Some of the risk for this product has been reduced via an increase in the minimum of the area measurement range, from 100 square meters up to 1000 square meters.

Table 5. VIIRS SRD prescribed requirements for the Active Fires product (TBD=to be determined; TBR=to be reviewed). Minimum area requirement has since increased to 1000 square meters.

SRD Parameter No.	Parameter	Threshold	Objective	Specification
	a. Horizontal Cell Size (HCS)			
N/A	1. At nadir	1 km (TBR)	0.5 km (TBR)	0.75 km
N/A	2. Worst case	2 km (TBR)	0.5 km (TBR)	1.6 km
N/A	b. Horizontal reporting interval	(TBD) (gapless or near gapless coverage of land areas required)	(TBD) (gapless or near gapless coverage of land areas required)	HCS
N/A	c. Horizontal coverage	Land	Land	Land
	d. Measurement range			
N/A	1. Sub-pixel average temperature of active fire	800 K – 1200 K	800 K – 1200 K	800 K – 1200 K
N/A	2. Sub-pixel area of active fire	From 100 m^2 to 50 m by greater of pixel in-scan and in-track dimensions (TBR)	From 50 m^2 to 100 m by greater of pixel in-scan and in-track dimensions (TBR)	From 1000 m^2 to 50 m by greater of pixel in-scan and in-track dimensions
	e. Measurement Uncertainty			
N/A	1. Sub-pixel average temperature of active fire	50 K (TBR)	25 K (TBR)	50 K
N/A	2. Sub-pixel area of active fire	30% (TBR)	15% (TBR)	30%
N/A	i. Minimum swath width (all other EDR thresholds met)	3000 km (TBR)	(TBR)	3000 km

3.4.2 Performance Metrics

The SRD requirements set the limits for an error budget in the Active Fires product. There is one key parameter in Table 5 that directly constrains the allowable errors in the Active Fires product: uncertainty, both for subpixel fire temperature and subpixel fire area. Appendix A of the VIIRS SRD defines the uncertainty metric for assessment of EDR algorithm performance.

Consider a single true value T of an EDR product at the product Horizontal Cell Size (HCS). A satellite-borne sensor will produce data which can be transformed through a retrieval algorithm into an estimate X_i of T, where the index i indicates that any arbitrary number N of such estimates can be made. Various error sources along the pipeline between the true value T and the measured value X_i will cause X_i to deviate from T.

The uncertainty U_{SRD} is defined in the VIIRS SRD as:

$$U_{\mathrm{SRD}} = \left(\frac{1}{N} \sum_{i=1}^{N} (X_i - \mu)^2 \right)^{1/2} \tag{2}$$

The uncertainty is therefore alternatively known as the root mean square (RMS) error between the measurements X_i and the true value T.

As mentioned in the SRD, the definition of uncertainty given in (2) is idealized, because it assumes a single value of T. In reality, (2) cannot be implemented, because there is an infinite number of possible values for T, each possible value is likely to be manifested as truth only once, and we cannot hope to pinpoint T to arbitrary accuracy.

The practical implementation of the SRD definition is to bin the possible values of T into small ranges that are large enough to provide a statistically significant number of test points, but small enough not to be dominated by natural variability. The simplest result is a modification of (2) into the following:

$$U = \left(\frac{1}{N} \sum_{i=1}^{N} (X_i - T_i)^2 \right)^{1/2} \tag{3}$$

Thus, the single value of T in the SRD uncertainty definition is now changed to the particular true value T_i corresponding to the measurement X_i. Equation (3) now exactly corresponds to the RMS error. This is a common statistical measure of algorithm performance. Interestingly, only the fire temperature and area are constrained by uncertainty requirements. No quality metric is assigned to fire detection. Were such a metric in place, it would best be couched in terms of a correct typing probability, similar to that for Surface Type or Snow Cover. In future versions of this ATBD, fire detection performance will be gauged in these terms for completeness.

3.4.3 Individual Error Sources for Investigation

The Active Fires product is subject to several sources of error. The sensitivity of the algorithm to these error sources was not explored in detail in Phase II, however they can be identified and briefly described here. Post-CDR algorithm development efforts should center around an assessment of these error sources in the context of the algorithm described in Section 3.3.

Sensor Errors

There are several key parameters associated with the VIIRS instrument that affect its ability to facilitate sound fire retrievals. These include calibration, sensor noise, saturation, spectral

content, geolocation, Modulation Transfer Function (MTF) effects, and band to band registration. Calibration will be handled post-launch via monitoring of gas flares and night-time volcanic flows, in much the same way MODIS is approaching the problem. Sensor noise in the VIIRS spectral bands is minimal due to the stringent requirements for Aerosol, Surface Temperature, and Ocean Color EDRs. This has led to a system design that is relatively low in noise all the way up to the temperatures encountered for typical fires. Saturation has already been discussed at length. Spectral content is superb for VIIRS; the reflectance-based bands that will be active at night are hoped to provide a new level of capability for temperature and area computations, or at least a complementary analysis capability. Geolocation and misregistration effects should be minimal due to the driving requirements for other EDRs, especially NDVI and Snow Cover, but coregistration is extremely important for fire retrievals, and so this issue must be thoroughly explored for the Active Fires Application. VIIRS will employ the MODIS/Landsat geolocation algorithm, which exhibits excellent performance after post-launch calibration. MTF effects in the imagery bands will be minimized by the Imagery EDR requirements, however these are not used in the baseline Active Fires algorithm. The MTF performance of the moderate resolution bands is somewhat looser, which actually helps from a saturation standpoint, but it also smears the signal being measured. This is particularly important in the presence of clouds. Each of these effects must be gauged and monitored as the VIIRS design evolves into fabrication, and the results should be recorded in future versions of this document.

Cloud Contamination

The presence of clouds can cause spurious signals in the MWIR that appear as fires if not properly accounted for. Threshold techniques are very sensitive to these effects. The VIIRS algorithm will benefit from a wealth of spectral data that are expected to minimize this error, and the VIIRS Cloud Mask is expected to be quite accurate by the time the first VIIRS is flown, because of the tremendous advances being made in cloud masking using MODIS data. At the least, the robustness of the "confident clear" category should be quite good for VIIRS, and this is the only category for which Active Fires performance is guaranteed. Performance in other situations will be evaluated as opportunities arise for a mature assessment.

Smoke

Smoke does not have a significant impact on LWIR signatures, however it will have a significant effect if SWIR bands are employed to mitigate saturation impacts. The effects of smoke on SWIR-derived brightness temperatures over fires still requires investigation, and the results of these analyses should be recorded in a future version of this document.

Bright Soils

The brightest surfaces in visible imagery are typically snow or desert sand. In the near infrared, dense vegetation is very bright. But in the SWIR and MWIR, soils are often the brightest surfaces, and in fact soils combined with erratic vegetation cover, such as in agriculture or savannas, can be bright enough in the MWIR to be mistaken for fires. Fortunately, VIIRS possesses a large amount of spectral information that can be used to filter out occurrences of bright soils or non-burning savannas, and the Quarterly Surface Types IP will also be of

assistance in this regard. Nevertheless, this effect will need to be quantified as part of the Active Fires error budget.

Sunglint

One would not expect a high frequency of fires over the oceans, where sunglint has an established reputation, but even a river or lake can exhibit enough sunglint to induce errors in a fire detection algorithm. Most fire detection algorithms incorporate a sunglint rejection routine. For VIIRS, this will be straightforward, since the Cloud Mask already contains two separate sunglint tests, and the output of these tests is made available to all downstream EDRs. Active Fires will therefore benefit from a system-level solution that must also satisfy the demanding needs of Ocean Color/Chlorophyll and Sea Surface Temperature users, and sunglint rejection should be quite effective at reducing errors in the detection and measurement of fires. The VIIRS land/sea mask will also be of great use in this endeavor.

Atmospheric Effects

The detection of fires relies primarily on the MWIR and LWIR bands, which unavoidably contain significant water vapor absorption features. CO_2 may also be a significant factor in band M13. As discussed in Section 3.3.2.1, atmospheric correction is a key step in the fire detection logic. It is expected that NCEP water vapor analyses will be of sufficient quality to make this error tolerable, but this will need to be verified. For the SWIR bands, water vapor absorption becomes significantly less important, but aerosol scattering plays an increased role. Once a strategy is established for correcting aerosol effects in the SWIR bands as part of fire temperature/area retrieval, sensitivity studies will be conducted to assess these errors.

Surface Heterogeneity

The phrase “background characterization” is often loosely used to describe a pivotal part of any fire detection algorithm, however this is not a trivial exercise, for the same reason that many land-based products carry significant uncertainty: surface heterogeneity. The background around an active fire is often not describable by a single parameter or surface type designation, and this leads to errors, especially in fire temperature and area computation. Surface heterogeneity will cause variability in both emissivity and background temperature, both of which are assumed to be known quantities in the application of (1). These effects will need to be assessed before a complete error budget can be constructed.

Natural Variability of Fires

Lastly, but certainly not the least important, are the variations in fires themselves. As already indicated earlier in this document, there are two general regimes for fires—smoldering and flaming. But the spread of temperatures for either scenario is significant. Flaming fires can range over hundreds of degrees K, and smoldering fires can range from 400 to 800 K. This kind of volatility will inevitably lead to some difficulty in pinning down the actual temperature and area, so that even the seemingly “simple” requirement of 50 K uncertainty in fire temperature becomes challenging. These kinds of errors, as with all other important sources of uncertainty, must be explored beyond Phase II using MODIS combined with higher-resolution satellite data.

3.4.4 Case Study (Fire Detection)

As a means of ensuring that we are moving forward with the best approach for fire detection, we tested our baseline contextual approach, along with a couple of other algorithms, on a case study from August of 2000 in Idaho and Montana. Figure 21 shows an image of some of the fires in question, from AVHRR data. A roughly corresponding set of fire polygons from the U.S. Forest Service is shown in Figure 22. We applied three different algorithms: the VIIRS baseline (contextual analysis); the pixel-based algorithm developed in Li et al. (2000); and a modification of the Li algorithm by Gong et al. (2001) that introduces some spatial contextual analysis. The tests in the three algorithms are summarized in Table 6. Their respective performances, shown as omission and commission errors at each step of the processing, are shown in Figure 23, Figure 24, and Figure 25. Numerical results are provided in Table 7. Note the significant reduction in commission errors when the NIR test is introduced into the VIIRS algorithm (it was already present in the Li and Gong techniques). All of the algorithms perform similarly in the final result, although the Gong algorithm still had more commission errors in the end. All three algorithms still require some work, but these results were sufficient to confirm our continued use of the VIIRS algorithm based on its extensive heritage and the extra robustness of spatial contextual analysis when applied to more than one case study.

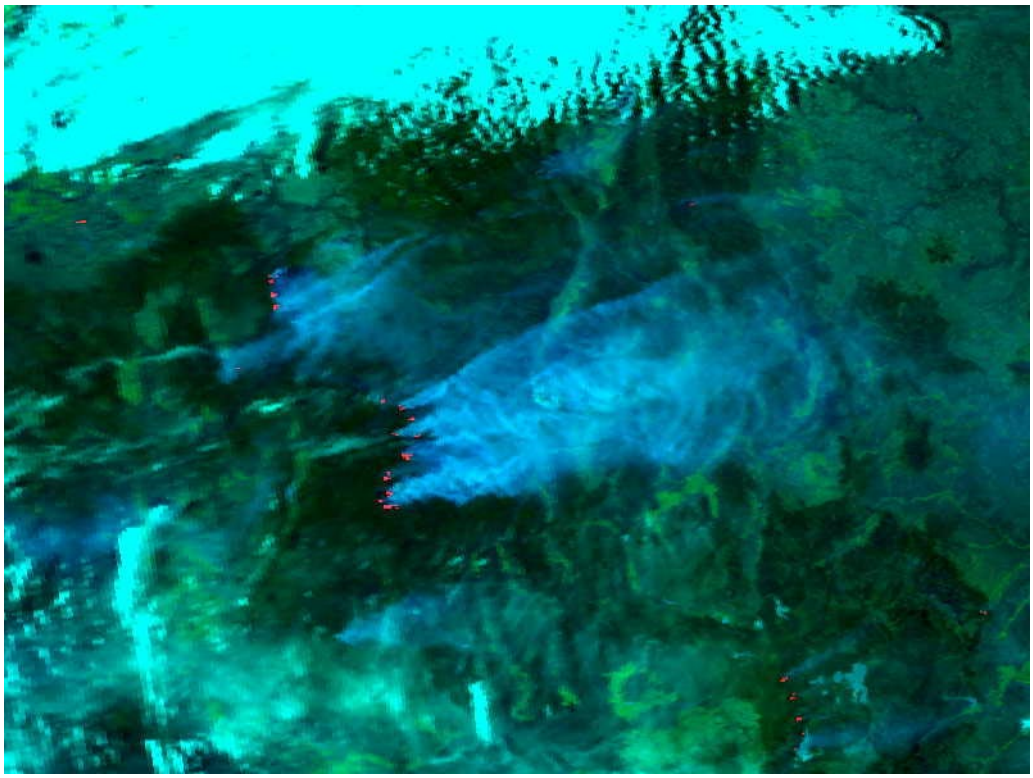

Figure 21. Wild fires in the Idaho/Montana area on August 29, 2000.

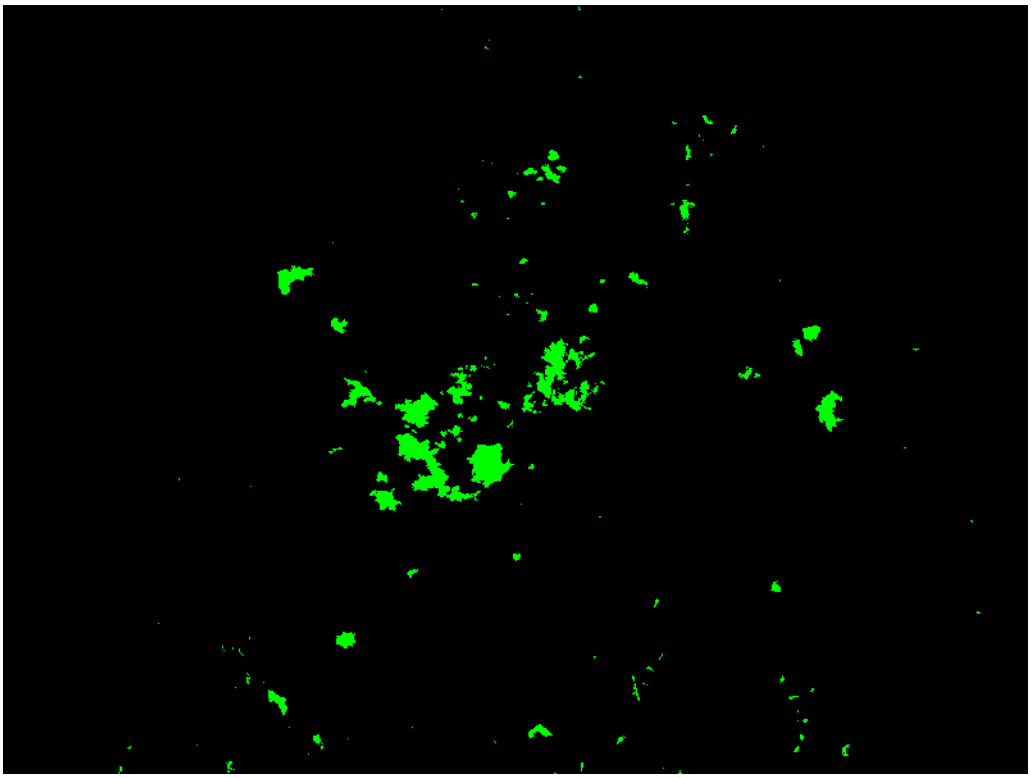

Figure 22. Fire polygons created by U.S. Forest Service for wild fires up to October 26, 2000.

Table 6. Comparison of three fire detection algorithms tested in case study.

Tests	Test Purpose	Fire Detection Algorithms		
		VIIRS Baseline (MODIS-like)	VIIRS Alternative 1 (Li)	VIIRS Alternative 2 (Gong)
1	Mask irrelevant pixels	Masking to eliminate water, snow/ice, urban, clouds, sunglint	Masking to eliminate cropland, grassland and water	Masking to eliminate water, urban, ag area, dune and desert
2	Label possible fire pixel	$T_4 > T_{4min}$ or $\Delta_{411} > \Delta_{411min}$	$T_4 > 315$ °K	$T_4 > 315$ °K
3	Remove thin clouds		$\Delta_{411} > 14$ °K	$\Delta_{411} >= 14$ °K
4	Remove Clouds		$T_{11} > 260$ °K	$T_{11} >= 260$ °K
5	Remote highly reflecting clouds & surface		$R_{nir} < 22\%$	$R_{nir} <= 22\%$
6	Background checking			$[22\% < R_{nir} <= 32\%]$ and $[R_{nir} < \mu_{Rnir\,3x3} - 1]$ or $T_4 > [\mu_{T4_3x3} + 5]$
7	Background checking	$f_{wxw} > f_{min}$ and $N_{wxw} > N_{min}$		
8	Remove thin clouds with warm background	$\{[(T_4 > \mu_4 + 4\sigma_4)$ or $(T_4 > T_{crit}]$ and $[(\Delta_{411} > \mu_{411} + 4\sigma_{411})$ or $(\Delta_{411} > \Delta_{crit}])$ or $(\Delta_{411} > \Delta_{abs}\}$	$\Delta_{1112} < 4.1$°K and $\Delta_{411} >= 19$°K	$\Delta_{1112} < 4$°K and $\Delta_{411} >= 19$°K
9				$R_{red} + R_{nir} <= 75\%$
10				$\lvert R_{red} - R_{nir} \rvert > 1\%$
11	Remove sub-pixel contamination	Sieve single fire pixels	Sieve single fire pixels	Sieve single fire pixels

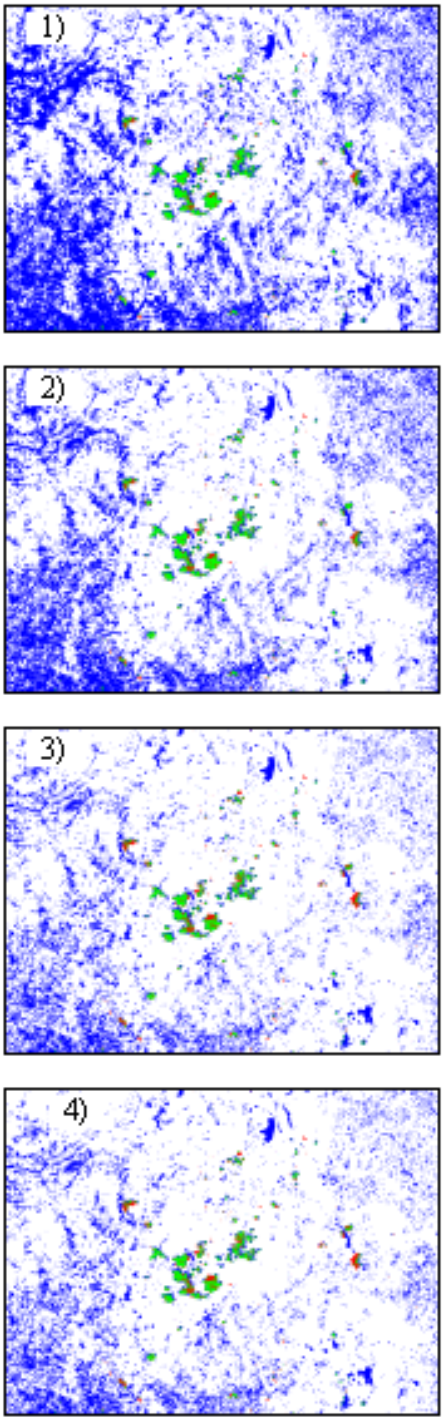

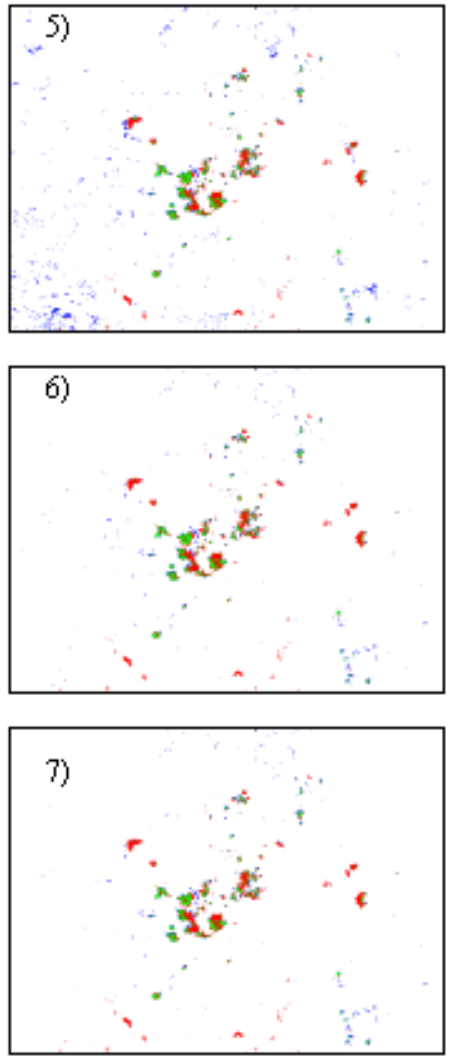

1) $T_4 > 315K$ and $\Delta_{411} > 14K$;
2) $[(R_{vis4} + R_{vis5}) > 120]$ or $[() > 80$ and $T_{12} < 285]$ or $[T_{12} < 265]$
3) $\{[(T_4 > \mu_4 + 4\sigma_4)$ or $(T_4 > T_{cold}]$ and $[(\Delta_{411} > \mu_{411} + 4\sigma_{411})$ or $(\Delta_{411} > \Delta_{cold}]\}$ or $\{\Delta_{411} > \Delta_{abs}\}$
4) $T_{11} > 260K$ CCRS(Li et al)
5) $R_{vis} < 22$; CCRS(Li et al)
6) *Forest* only. CCRS(Li et al)
7) $\Delta_{1112} < 4K$ and $\Delta_{411} >= 19K$. CCRS(Li et al)

Green – Correctly detected fire pixels, Blue – Commission Error, Red – Omission Error

Figure 23. Step-by-step performance of VIIRS fire detection algorithm for Idaho/Montana case study.

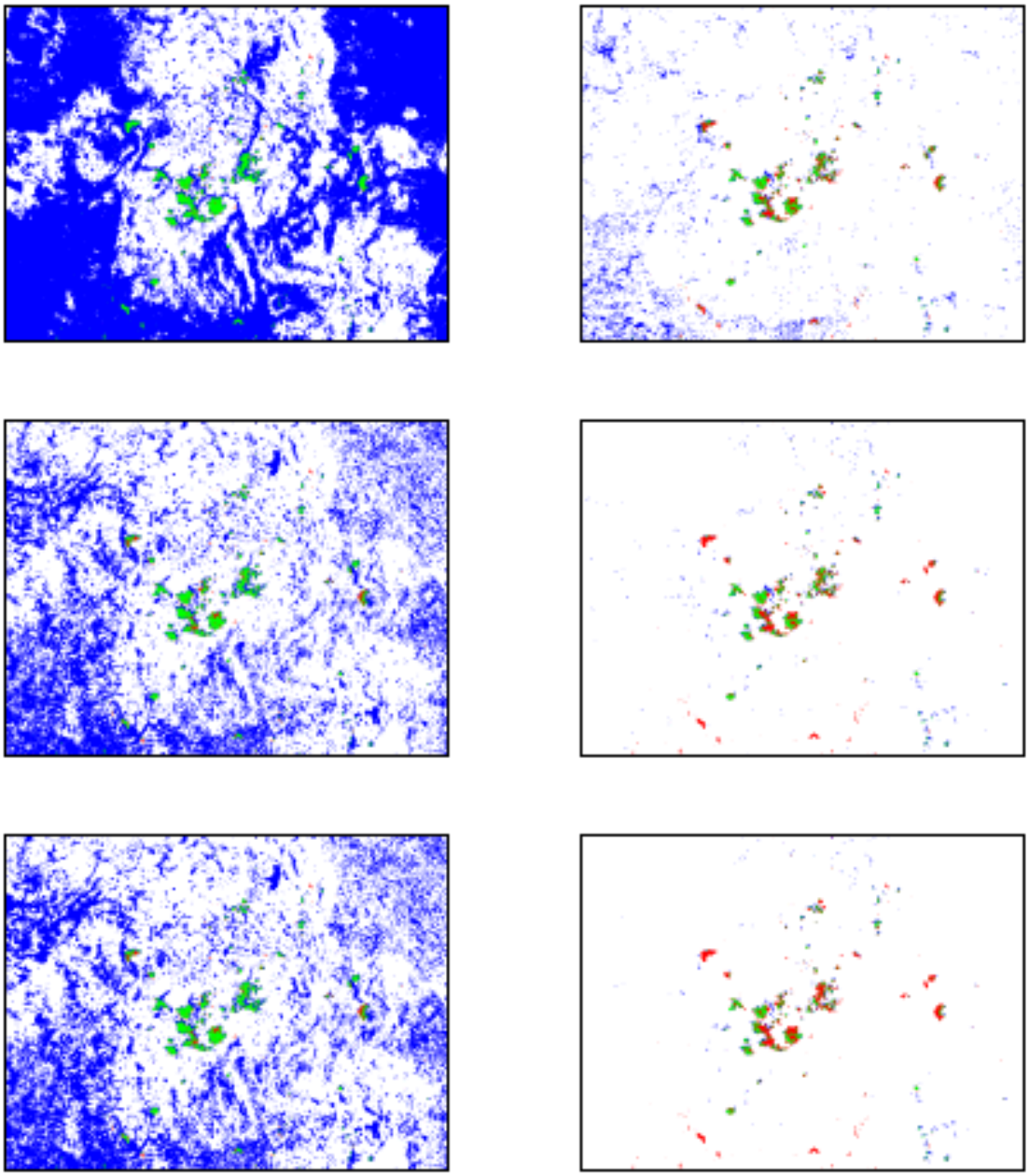

1) $T_a > 315$ °K
2) $\Delta_{a11} > 14$ °K
3) $T_{11} > 260$ °K
4) $R_{vis} < 22\%$
5) *Surface Type* = *Forest* only
6) $\Delta_{1112} < 4.1$°K and $\Delta_{a11} >= 19$°K

Figure 24. Step-by-step performance of Li et al. (2000) fire detection algorithm for Idaho/Montana case study.

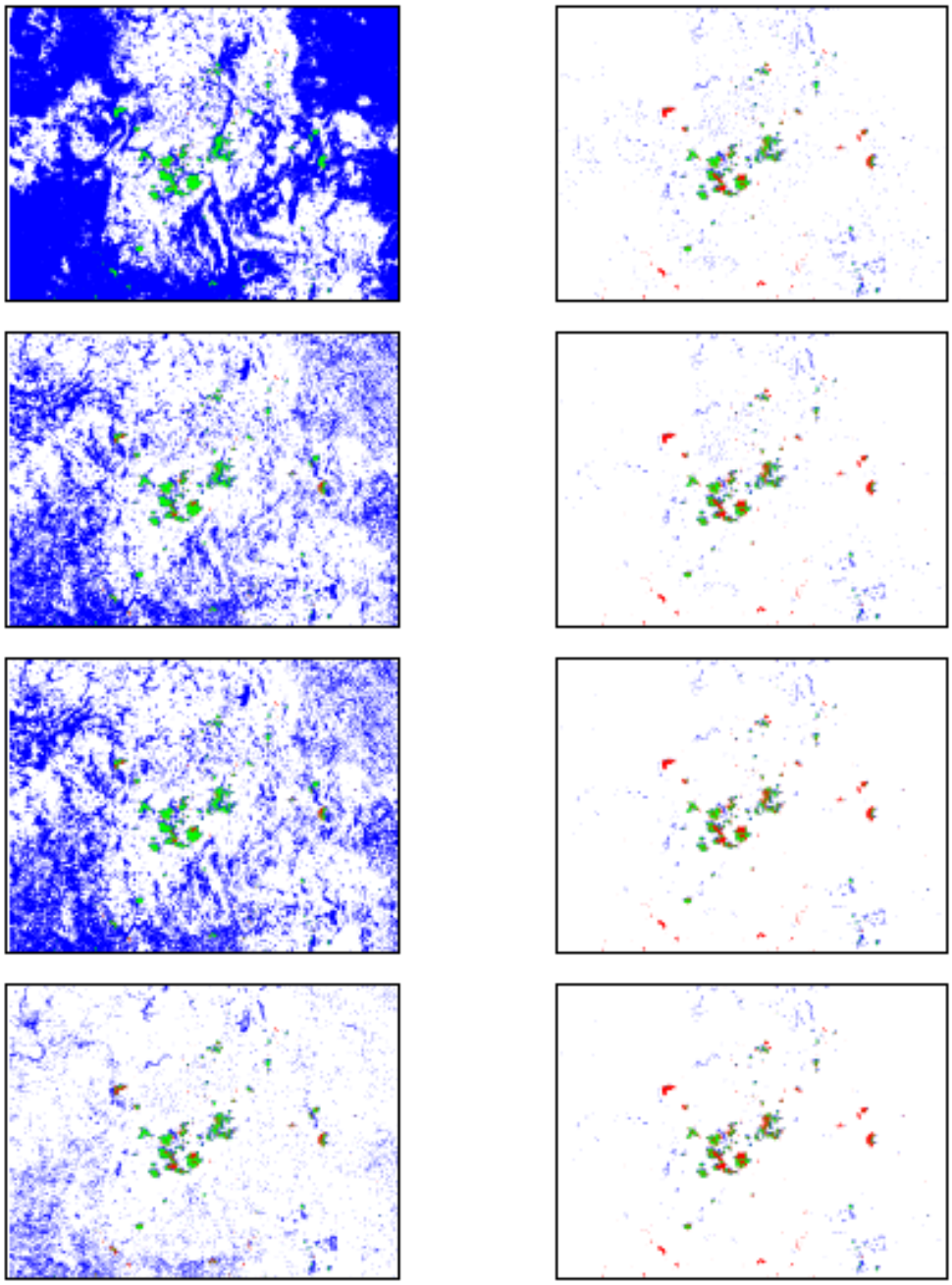

1) $T_a > 315\,^{\circ}K$
2) $\Delta_{a11} > 14\,^{\circ}K$
3) $T_{11} > 260\,^{\circ}K$
4) $[R_{nir} < 22\%]$ or $\{[(22\% < R_{nir} <= 32\%)$ and $(R_{nir} < \mu_{nir_ref} - 1)]$ or $[T_a > (\mu_{ta_ref} + 5)]\}$
5) *Surface Type* = *Forest* only
6) $\Delta_{1111} < 4\,^{\circ}K$ and $\Delta_{a11} >= 19\,^{\circ}K$
7) $R_{red} + R_{nir} <= 75\%$
8) $|R_{red} - R_{nir}| > 1\%$

Figure 25. Step-by-step performance of Gong et al. (2001) fire detection algorithm for Idaho/Montana case study.

Table 7. Quantitative assessment of fire detection algorithms' performance in case study.

1-VIIRS (MODIS-like) ...

step	Num_fire	TrueFire	%	ComError	%	OmnError	%		
0	139720	5698	81.7	134022	1922.6	1273	18.3	1940.8	Before Sieve
1	98740	5395	77.4	93345	1339.0	1576	22.6	1361.7	
2	64033	4664	66.9	59369	851.7	2307	33.1	884.8	
3	64033	4664	66.9	59369	851.7	2307	33.1	884.8	
4	7019	2797	40.1	4222	60.6	4174	59.9	120.4	
5	4337	2561	36.7	1776	25.5	4410	63.3	88.7	
6	4196	2522	36.2	1674	24.0	4449	63.8	87.8	
step	Num_fire	TrueFire	%	ComError	%	OmnError	%		After Sieve
0	138290	5696	81.7	132594	1902.1	1275	18.3	1920.4	
1	97096	5391	77.3	91705	1315.5	1580	22.7	1338.2	
2	61966	4656	66.8	57310	822.1	2315	33.2	855.3	
3	61966	4656	66.8	57310	822.1	2315	33.2	855.3	
4	6729	2772	39.8	3957	56.8	4199	60.2	117.0	
5	4212	2531	36.3	1681	24.1	4440	63.7	87.8	
6	4084	2490	35.7	1594	22.9	4481	64.3	87.1	

Time used by this method: 27.0 seconds

3-Li et al ...

step	Num_fire	TrueFire	%	ComError	%	OmnError	%	
0	277290	6480	93.0	270810	3884.8	491	7.0	3891.9
1	139784	5698	81.7	134086	1923.5	1273	18.3	1941.7
2	131825	5628	80.7	126197	1810.3	1343	19.3	1829.6
3	18218	3766	54.0	14452	207.3	3205	46.0	253.3
4	5575	3192	45.8	2383	34.2	3779	54.2	88.4
5	4254	2544	36.5	1710	24.5	4427	63.5	88.0
step	Num_fire	TrueFire	%	ComError	%	OmnError	%	
0	276657	6479	92.9	270178	3875.7	492	7.1	3882.8
1	138358	5696	81.7	132662	1903.1	1275	18.3	1921.3
2	130374	5626	80.7	124748	1789.5	1345	19.3	1808.8
3	17310	3751	53.8	13559	194.5	3220	46.2	240.7
4	5380	3172	45.5	2208	31.7	3799	54.5	86.2
5	4137	2512	36.0	1625	23.3	4459	64.0	87.3

Time used by this method: 9.0 seconds

4-Li et al Tuned

step	Num_fire	TrueFire	%	ComError	%	OmnError	%	
0	185852	6091	87.4	179761	2578.7	880	12.6	2591.3
1	91888	5603	80.4	86285	1237.8	1368	19.6	1257.4
2	88963	5558	79.7	83405	1196.5	1413	20.3	1216.7
3	18290	3019	43.3	15271	219.1	3952	56.7	275.8
4	3532	2426	34.8	1106	15.9	4545	65.2	81.1
5	2958	2045	29.3	913	13.1	4926	70.7	83.8
step	Num_fire	TrueFire	%	ComError	%	OmnError	%	
0	185387	6089	87.3	179298	2572.1	882	12.7	2584.7
1	90728	5600	80.3	85128	1221.2	1371	19.7	1240.8
2	87798	5555	79.7	82243	1179.8	1416	20.3	1200.1
3	17480	2993	42.9	14487	207.8	3978	57.1	264.9
4	3423	2399	34.4	1024	14.7	4572	65.6	80.3
5	2893	2015	28.9	878	12.6	4956	71.1	83.7

Time used by this method: 9.0 seconds

5-Gong et al.

step	Num_fire	TrueFire	%	ComError	%	OmnError	%	
0	277290	6480	93.0	270810	3884.8	491	7.0	3891.9
1	139784	5698	81.7	134086	1923.5	1273	18.3	1941.7
2	131825	5628	80.7	126197	1810.3	1343	19.3	1829.6
3	39353	4701	67.4	34652	497.1	2270	32.6	529.7
4	11666	3934	56.4	7732	110.9	3037	43.6	154.5
5	8585	3389	48.6	5196	74.5	3582	51.4	125.9
6	6929	3250	46.6	3679	52.8	3721	53.4	106.2
7	6396	3015	43.3	3381	48.5	3956	56.7	105.3
step	Num_fire	TrueFire	%	ComError	%	OmnError	%	
0	276657	6479	92.9	270178	3875.7	492	7.1	3882.8
1	138358	5696	81.7	132662	1903.1	1275	18.3	1921.3
2	130374	5626	80.7	124748	1789.5	1345	19.3	1808.8
3	35105	4689	67.3	30416	436.3	2282	32.7	469.1
4	10022	3919	56.2	6103	87.5	3052	43.8	131.3
5	7796	3372	48.4	4424	63.5	3599	51.6	115.1
6	6661	3232	46.4	3429	49.2	3739	53.6	102.8
7	6115	2986	42.8	3129	44.9	3985	57.2	102.1

Time used by this method: 51.0 seconds

3.5 PRACTICAL CONSIDERATIONS

3.5.1 Numerical Computation Considerations

Paragraph SRDV3.2.1.5.4-1 of the VIIRS SRD states the following:

> *"The scientific SDR and EDR algorithms delivered by the VIIRS contractor shall be convertible into operational code that is compatible with a 20 minute maximum processing time at either the DoD Centrals or DoD field terminals for the conversion of all pertinent RDRs into all required EDRs for the site or terminal, including those based wholly or in part on data from other sensor suites."*

RDR here stands for Raw Data Record. This essentially means that any and all EDRs must be completely processed from VIIRS raw data, including calibration and georeferencing, within 20 minutes from the time the raw data are available. This requirement is a strong reminder that VIIRS is an operational instrument.

The Active Fires product exists primarily as a science requirement, however its operational utility is clear, and the HSS and MODIS Rapid Response System provide excellent examples of operational fire monitoring. The kinds of branching decisions involved in the fire detection algorithm can have a more significant impact on computing time than one might first expect, however it is expected that the VIIRS coding effort will produce code that is efficient enough to be used operationally.

3.5.2 Programming and Procedural Considerations

The VIIRS Active Fires code will be developed in concert with developments from MODIS, and its operational aspects will be patterned as much as possible from the HSS processing architecture. These two heritages should reduce the need for extensive programming and procedural resources for the VIIRS Active Fires product. VIIRS Phase II efforts are largely software-focused, and the methodology for this development work is based on sound and proven principles, as discussed in the VIIRS Algorithm Software Development Plan *[Y6635]*. The present maturity of the VIIRS software is detailed in the VIIRS Algorithm Software Maturity Assessment document *[Y6661]*. The maturity and remaining Phase II tasks for the algorithms themselves is summarized in the VIIRS Algorithm/Data Processing Technical Report *[Y7040]*. The software designs relevant to Active Fires are summarized in the VIIRS Context Level Software Architecture *[Y2469]*, Land Module Level Software Architecture *[Y2474]*, Land Module Level Detailed Design *[Y2483]*, and Active Fires Unit Level Detailed Design *[Y3283]*. These designs will be tested at the system level as described in the most recent versions of the VIIRS Software Integration and Test Plan *[Y3236]*, Algorithm Verification and Validation Plan *[Y3237]*, and System Verification and Validation Plan *[Y3270]*. A summary of the ultimate strategy for operational application of the system of VIIRS algorithms is provided in the VIIRS Operations Concept document *[Y2468]*. The VIIRS Interface Control Document (ICD *[Y2470]*) provides more detail on the specifics of ancillary data requirements for Active Fires and other VIIRS products.

3.5.3 Configuration of Retrievals

The Active Fires Application will be configured in tune with the Land Quality Flag (LQF) output appended to the VIIRS Surface Reflectance IP. The reader is directed to *[Y2411]* for a complete description of the LQF structure, which applies to all land products. Active Fires output will be reported for all pixels that are not confidently cloudy.

3.5.4 Quality Assessment and Diagnostics

While the LQF output will be the primary descriptor of the Active Fires Application quality, it will be necessary from time to time to run diagnostics on overall algorithm performance, particularly to track calibration behavior in M13, which will not be calibrated for the high radiance range until post-launch observations of gas flares and volcanic flows are available. Future versions of this document should include plans for carrying out these activities, once the entire NPP, NPOESS, and VIIRS calibration and validation plans have been more thoroughly mapped out.

3.5.5 Exception Handling

Where the LQF output indicates Active Fires should not be retrieved, the EDR fields will be filled with predefined "missing" values. The primary causes of such flagging would be the presence of cloud or extremely heavy aerosol (which itself could indicate fire nearby, of course), or pixels located over ocean or sea ice.

3.6 ALGORITHM VALIDATION

Validation of the VIIRS Active Fires product will follow the lead of validation from MODIS efforts. Extensive pre-launch campaigns are already available, including MODIS Airborne Simulator (MAS) scenes such as those from the Smoke, Clouds, and Radiation (SCAR) campaigns. NASA intensive field programs in South America and Africa are being conducted and will continue into the MODIS era, and EOS test sites are established in part to deal with the investigation of fires. In particular, campaigns like Southern African Regional Science Initiative (SAFARI) 2000 have provided and will continue to provide excellent test data sets for development and refinement of the algorithms presented here. MODIS, AVHRR, and GOES also provide platforms for algorithm testing. Coincident use of Advanced Spaceborne Thermal Emission and Reflection Radiometer (ASTER) and MODIS data from Terra and Aqua should further reduce algorithmic risk. Development of a detailed validation plan for Active Fires products is strongly recommended, once experience has been gained from MODIS efforts and the overall calibration/validation plan for NPP and NPOESS has been refined.

4.0 ASSUMPTIONS AND LIMITATIONS

4.1 ASSUMPTIONS

The following assumptions are made with respect to the retrievals described in this document:

1) The VIIRS Cloud Mask functions at a high level of accuracy, including the treatment of cirrus and the identification of sunglint

2) The VIIRS reflective bands at 865 nm, 1.24 µm, 1.61 µm, and 2.25 µm will be active at night (this is in fact the case in the system and sensor specifications)

3) Dual gain will be implemented for the 4.05 µm band to decouple Fires from Sea Surface Temperature, since the latter would take precedent in any inter-algorithm trades

4) The saturation values for each of the bands associated with the Active Fires product will be retained at their current levels or increased

4.2 LIMITATIONS

The following limitations apply to the at-launch retrievals of described in this document:

1) Active Fires retrievals in the presence of extreme aerosol loading or smoke will be questionable, and spec performance is not guaranteed in these circumstances.

2) Active Fires retrievals for broken clouds (where the central pixel is considered clear or probably clear) may suffer from MTF effects that drive performance below spec; this has not yet been established either way

3) The maturity of using the SWIR bands is quite low at this writing, and must therefore be considered a source of significant risk with regard to system performance

5.0 REFERENCES

Andreae, M. O., (1991). Biomass burning: its history, use, and distribution and its impact on environmental quality and global climate. In: Global Biomass Burning, p.3-21, *J. S. Levine (Ed.). Cambridge, MA: The MIT Press.*

Barbosa, P.M., J.-M. Gregoire, and J.M.C. Pereira, 1997: Detection of burned areas in Africa using a multitemporal multithreshold analysis of NOAA-AVHRR-GAC data. *Earth Surface Remote Sensing*, edited by Giovanna Cecchi et al., Proceedings of SPIE Vol. 3222, pp. 67-75, SPIE, Bellingham, Washington.

Dozier, J. (1981). A method for satellite identification of surface temperature fields of subpixel resolution, *Remote Sensing of Environment*, 11, 221-229.

Elvidge, C.D., 1997: *Wildfire detection with meteorological satellite data: results from New Mexico during June of 1996 using GOES, AVHRR, and DMSP-OLS.* Report to NOAA-NESDIS, June 16, 1997.

Eva, H.D., and E.F. Lambin, 1998: Burnt area mapping in Central Africa using ATSR data, *International Journal of Remote Sensing*, 19, 3473-3497.

Fernandez, A., P. Illera, and J.L. Casanova, 1997: Automatic mapping of surfaces affected by forest fires in Spain using AVHRR NDVI composite data. *Remote Sensing of Environment*, 60, 153-162.

Flasse, S.P., and P. Ceccato, 1996: A contextual algorithm for AVHRR fire detection. *International Journal of Remote Sensing*, 17, 419-424.

Franca, J-R, J-M Brustet, J. Fontan, J-M Gregoire and J. P. Malinggreau (1993). A Multi-spectral remote sensing of biomass burning in West Africa During 90/91 Dry season, Presented at the XVM-EGS General Assembly, May 1993, Wiesbaden, Germany.

Franca, J. Ricardo De A., J.-M. Brustet, and J. Fontan, 1995: Multispectral remote sensing of biomass burning in West Africa. *Journal of Atmospheric Chemistry*, 22, 81-110.

Giglio, L., and J. D. Kendall (2000). Application of the Dozier retrieval to wildfire characterization: a sensitivity analysis. Submitted to *Remote Sensing of Environment*.

Harris, A.J.L., 1996: Towards automated fire monitoring from space: semi-automated mapping of the January 1994 New South Wales wildfires using AVHRR data. *International Journal of Wildland Fire*, 6, 107-116.

IPO (2000). Visible/Infrared Imager/Radiometer Suite (VIIRS) Sensor Requirements Document (SRD) for National Polar-Orbiting Operational Environmental Satellite System (NPOESS) spacecraft and sensors, Rev. 2b/c. Prepared by Assoc. Directorate for Acquisition, NPOESS Integrated Program Office, Silver Spring, MD.

Justice, C.O., and P. Dowty (1993), *IGBP-DIS satellite fire detection algorithm workshop technical report*, IGBP-DIS Working Paper No. 9, 88 pp., Feb. 1993, NASA/GSFC, Greenbelt, Maryland.

Kasischke, E.S. and N.H.F. French, 1995: Locating and estimating the areal extent of wildland fires in Alaskan boreal forests using multiple-season AVHRR NDVI composite data. *Remote Sensing of Environment*, 51, 263-265.

Kaufman, Y., and C. Justice, 1998: *MODIS Fire Products Algorithm Technical Background Document*, Version 2.2, EOS ID #2741.

Kaufman, Y. J., R. G. Kleidman, and M. D. King (1998). SCAR-B fires in the tropics: Properties and remote sensing from EOS-MODIS. *J. Geophys. Res*., 103, 31955-31968.

Kaufman, Y. J., P. V. Hobbs, V. W. J. H. Kirchoff, P. Artaxo, L. A. Remer, B. N. Holben, M. D. King, D. E. Ward, E. M. Prins, K. M. Longo, L. F. Mattos, C. A. Nobre, J. D. Spinhirne, Q. Ji, A. M. Thompson, J. F. Gleason, S. A. Christopher, and S. –C. Tsay (1998). Smoke, Clouds, and Radiation-Brazil (SCAR-B) experiment. *J. Geophys. Res*., 103, 31737-31808.

Kaufman, Y. J., A. Setzer, C. Justice, C. J. Tucker, M. C. Pereira and I. Fung. (1990). Remote Sensing of Biomass Burning in the Tropics, In: Fire in the Tropical Biota: Ecosystem Processes and Global challenges, J. G. Goldammer (ed.), Springer-Verlag, Berlin, pp371-399.

Lee, T.F., and P. M. Tag, 1990: Improved detection of hotspots using the AVHRR 3.7 mm channel. *Bulletin of the American Meteorological Society*, 71, 1722-1730.

Levine, J. S.(1991). Global biomass burning: atmospheric, climatic, and biospheric implications, In:. Global Biomass Burning, p.3-21, *J. S. Levine (Ed.). Cambridge, MA: The MIT Press.*

Li, Z., S. Nadon, and J. Cihlar, 2000: Satellite detection of Canadian boreal forest fires: Development and application of an algorithm. *International Journal of Remote Sensing*, 21, 57-69.

Martin, P., and E. Chuvieco, 1993: Mapping and evaluation of burned land from multitemporal analysis of AVHRR NDVI images. *Proc. International Workshop on Satellite Technology and GIS for Mediterranean Forest Mapping and Fire Management*, Department of Forestry and Natural Environment, Aristotle University, Thessaloniki, Greece, pp. 71-83.

Matson, M., and J. Dozier, 1981: Identification of subresolution high temperature sources using a thermal IR sensor. *Photogrammetric Engineering and Remote Sensing*, 47, 1311-1318.

Matson, M., S.R. Schneider, B. Aldridge, and B. Satchwell, 1984: *Fire detection using the NOAA (National Oceanic and Atmospheric Administration)-series satellites*. NOAA Technical Report NESDIS 7, available from the National Technical Information Service, Springfield, VA 22161.

Matson, M., and B. Holben, 1987: Satellite detection of tropical burning in Brazil. *International Journal of Remote Sensing*, 8, 509-516.

Melinotte, J.M., and O. Arino, 1995: *The Ionia '1-km' Net-Browser experience: quicklook processing and assess statistics*. EOQ, No. 50, Dec. 1995.

Pereira, A., and A.W. Setzer , 1993: Spectral characteristics of fire scars in Landsat-5 TM images of Amazonia. *International Journal of Remote Sensing*, 14, 2061-2078.

Pereira, M. C. and A. W. Setzer (1993a). Spectral characteristics of deforestation fires in NOAA/AVHRR images, *Int. J. Remote Sensing*, 14, 583-597.

Planet, W.G. (ed.), (1988). Data extraction and calibration of TIROS-N/NOAA radiometers. NOAA Technical Memorandum NESS 107 – Rev. 1, Oct. 1988. 130 pp.

Pozo, D., F.J. Olmo, and L. Alados-Arboledas, 1997: Fire detection and growth monitoring using a multitemporal technique on AVHRR mid-infrared and thermal channels. *Remote Sensing of Environment*, 60, 111-120.

Press, W.H., B.P. Flannery, S.A.Teukolsky, and W.T. Vetterling, 1989: *Numerical recipes: the art of scientific computing*. Cambridge University Press, 702 pp.

Prins, E.M., and W.P. Menzel, 1992: Geostationary satellite detection of biomass burning in South America. *International Journal of Remote Sensing*, 13, 2783-2799.

Prins, E.M., and W.P. Menzel, 1996a: Monitoring fire activity in the western hemisphere with the new generation of geostationary satellite. *AMS 22nd Conference of Agricultural and Forest Meteorology with Symposium on Fire and Forest Meteorology*, Atlanta, GA, Jan. 28-Feb.2, 1996, p.272-275.

Prins, E.M., and W.P. Menzel, 1996b: Monitoring biomass burning and aerosol loading and transport from a geostationary satellite perspective. *AMS 7th Symposium on Global Change Studes*, Atlanta GA, Jan.28-Feb.2, 1996.

Raytheon Hazard Support System, 1998: *Civil sensor fire, volcanoes, and volcanic ash cloud detection algorithm trade study*, Revision 1, CDRL A004, Technical Report #14.

Roy, D.P., L. Giglio, J.K. Kendall, and C.O. Justice, 1999: Multitemporal active-fire based burn scar detection algorithm. *International Journal of Remote Sensing*, 20, 1031-1038.

Saunders and Kriebel, 1988: An improved method for detecting clear-sky and cloud radiance from AVHRR data. *International Journal of Remote Sensing*, 9, 120-150.

Setzer, A.W., and M.C. Pereira, 1991: Operational detection of fires in Brazil with NOAA-AVHRR, presented at the *24th International Symposium on Remote Sensing of Environment*, Rio de Janeiro, Brazil, 27-31 May 1991.

Vickos, J.B., 1991: Télédétection des feux de savanes en Afrique Intertropicale et estimation des emissions de constituents ayant un interêt atmosphérique, (in French), Thèse de doctorate de l'Univ., Paul Sabatier, Toulouse, France.